

# Combining Pseudo-Point and State Space Approximations for Sum-Separable Gaussian Processes

Will Tebbutt<sup>1</sup>

Arno Solin<sup>2</sup>

Richard E. Turner<sup>1</sup>

<sup>1</sup>University of Cambridge, UK

<sup>2</sup>Aalto University, Finland

## Abstract

Gaussian processes (GPs) are important probabilistic tools for inference and learning in spatio-temporal modelling problems such as those in climate science and epidemiology. However, existing GP approximations do not simultaneously support large numbers of off-the-grid spatial data-points and long time-series which is a hallmark of many applications. Pseudo-point approximations, one of the gold-standard methods for scaling GPs to large data sets, are well suited for handling off-the-grid spatial data. However, they cannot handle long temporal observation horizons effectively reverting to cubic computational scaling in the time dimension. State space GP approximations are well suited to handling temporal data, if the temporal GP prior admits a Markov form, leading to linear complexity in the number of temporal observations, but have a cubic spatial cost and cannot handle off-the-grid spatial data. In this work we show that there is a simple and elegant way to combine pseudo-point methods with the state space GP approximation framework to get the best of both worlds. The approach hinges on a surprising conditional independence property which applies to space–time separable GPs. We demonstrate empirically that the combined approach is more scalable and applicable to a greater range of spatio-temporal problems than either method on its own.

## 1 INTRODUCTION

Large spatio-temporal data containing millions or billions of observations arise in various domains, such as climate science. While Gaussian process (GP) models [Rasmussen and Williams, 2006] can be useful models in such settings, the computational expense of exact inference is typically

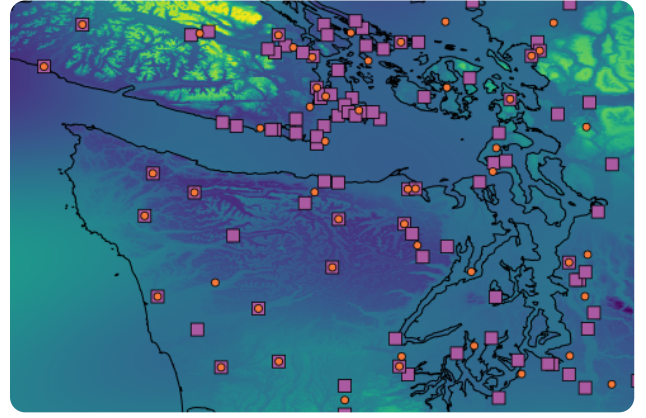


Figure 1: Spatial slice of a large-scale spatio-temporal modelling problem: The posterior mean belief over max temperature (standardised scale,  $-3$  to  $3$ ) on a day in early 2020 around Seattle and Vancouver. Pink squares are weather stations, orange dots are pseudo-points.

prohibitive, necessitating approximation. This work combines two classes of approximations with complementary strengths and weaknesses to tackle spatio-temporal problems: pseudo-point [Quiñonero-Candela and Rasmussen, 2005, Bui et al., 2017] and state-space [Särkkä et al., 2013, Särkkä and Solin, 2019] approximations. Fig. 1 shows a single time-slice of a spatio-temporal model for daily maximum temperature, which extrapolates from fixed weather stations, constructed using this technique.

This work hinges on a conditional independence property possessed by separable GPs. This property was identified by O’Hagan [1998], and appears to have gone largely unnoticed within the GP community. This property, in conjunction with the imposition of some structure on the pseudo-point locations, yields a collection of methods for approximate inference algorithm which scale linearly in time, the same as standard pseudo-point methods in space, and which can be implemented straightforwardly by utilising standard Kalman filtering-like algorithms.

In particular, we show (i) how O’Hagan’s conditional independence property can be exploited to significantly accelerate the variational inference scheme of Titsias [2009] for GPs with separable and sum-separable kernels, (ii) how this can be straightforwardly combined with the Markov property exploited by state space approximations [Särkkä and Solin, 2019] to obtain an accurate approximate inference algorithm for sum-separable spatio-temporal GPs that scales linearly in time, and (iii) how the earlier work of Hartikainen et al. [2011] on this topic is more closely related to the pseudo-point work of Csató and Oppér [2002] and Snelson and Ghahramani [2005] than previously realised.

## 2 SUM-SEPARABLE SPATIO-TEMPORAL GPs

We call a GP *separable across space and time* if its kernel is of the form

$$\kappa((\mathbf{r}, \tau), (\mathbf{r}', \tau')) = \kappa^{\mathbf{r}}(\mathbf{r}, \mathbf{r}') \kappa^{\tau}(\tau, \tau') \quad (1)$$

where  $\mathbf{r}, \mathbf{r}' \in \mathcal{X}$  are spatial inputs and  $\tau, \tau' \in \mathbb{R}$  are temporal inputs. We also call kernels such as  $\kappa$  separable. There is no particular restriction on what we define  $\mathcal{X}$  to be – it could be 3-dimensional Euclidean space in the literal sense, or it could be something else, such as a graph or the surface of a sphere. Moreover, we place no restrictions on the form of  $\kappa^{\mathbf{r}}$ , in particular we do not require it to be separable. Similarly, while the temporal inputs must be in  $\mathbb{R}$ , it is irrelevant whether this dimension actually corresponds to time or to something else entirely.

This work considers a generalisation of separable GPs that we call *sum-separable across space and time*, or simply *sum-separable*. We call a GP *sum-separable* if it can be sampled by summing samples from a collection of independent separable GPs. Specifically, let  $f_p \sim \mathcal{GP}(0, \kappa_p)$ ,  $p = \{1, \dots, P\}$ , be a collection of  $P$  independent separable GPs with kernels  $\kappa_p$ , and  $f := \sum_{p=1}^P f_p$ , then  $f$  is sum-separable.  $f$  has kernel

$$\kappa((\mathbf{r}, \tau), (\mathbf{r}', \tau')) = \sum_{p=1}^P \kappa_p((\mathbf{r}, \tau), (\mathbf{r}', \tau')), \quad (2)$$

which is *not* separable, meaning that sum-separable GPs such as  $f$  are not generally separable. In fact they are a much more expressive family of models, as they can represent processes which vary on multiple length scales in space and time. Note that these are also distinct from additive GPs [Duvenaud et al., 2011] since each function depends on both space and time.

## 3 PSEUDO-POINT APPROXIMATIONS

Pseudo-point approximations tackle the scaling problems of GPs by summarising a complete data set through a

much smaller set of carefully-chosen uncertain pseudo-observations.

Consider a GP,  $f \sim \mathcal{GP}(m, \kappa)$ , of which  $N$  observations  $\mathbf{y} \in \mathbb{R}^N$  are made at locations  $\mathbf{x} \in \mathcal{X}^N$  through observation model  $p(\mathbf{y} | \mathbf{f}) = \prod_{n=1}^N p(\mathbf{y}_n | \mathbf{f}_n)$ ,  $\mathbf{f}_n := f(\mathbf{x}_n)$ . The seminal work of Titsias [2009], revisited by Matthews et al. [2016], introduced the following approximation to the posterior distribution over  $f$ :

$$q(f) = q(\mathbf{u}) p(f_{\neq \mathbf{u}} | \mathbf{u}), \quad (3)$$

where  $\mathbf{u}_m := f(\mathbf{z}_m)$  are the *pseudo-points* for a collection of  $M$  *pseudo-inputs*  $\mathbf{z}_{1:M}$ , and  $f_{\neq \mathbf{u}} := f \setminus \mathbf{u}$  are all of the random variables in  $f$  except those used as pseudo-points. We assume that  $q(\mathbf{u})$  is Gaussian with mean  $\mathbf{m}_{\mathbf{u}}^q$  and covariance matrix  $\mathbf{C}_{\mathbf{u}}^q$ . Subject to the constraint imposed in Eq. (3), this family contains the optimal choice for  $q(\mathbf{u})$  if each observation model  $p(\mathbf{y}_n | f(\mathbf{x}_n))$  is Gaussian; moreover, a Gaussian form for  $q(\mathbf{u})$  is the de-facto standard choice when  $p(\mathbf{y}_n | f(\mathbf{x}_n))$  is not Gaussian – see e.g. Hensman et al. [2013]. This choice for  $q(\mathbf{u})$  yields the following approximate posterior predictive distribution at any collection of test points  $\mathbf{x}_*$

$$q(\mathbf{f}_*) = \mathcal{N}(\mathbf{f}_*; \mathbf{C}_{\mathbf{f}_* \mathbf{u}} \Lambda_{\mathbf{u}} \mathbf{m}_{\mathbf{u}}^q, \mathbf{C}), \quad (4)$$

$$\mathbf{C} := \mathbf{C}_{\mathbf{f}_*} - \mathbf{C}_{\mathbf{f}_* \mathbf{u}} \Lambda_{\mathbf{u}} \mathbf{C}_{\mathbf{u} \mathbf{f}_*} + \mathbf{C}_{\mathbf{f}_* \mathbf{u}} \Lambda_{\mathbf{u}} \mathbf{C}_{\mathbf{u}}^q \Lambda_{\mathbf{u}} \mathbf{C}_{\mathbf{u} \mathbf{f}_*},$$

where  $\Lambda_{\mathbf{u}} := \mathbf{C}_{\mathbf{u}}^{-1}$  is the inverse of the covariance matrix between all pseudo-points,  $\mathbf{C}_{\mathbf{f}_* \mathbf{u}}$  is the cross-covariance between the prediction points and pseudo-points under  $f$ , and  $\mathbf{m}_{\mathbf{u}}$  and  $\mathbf{m}_{\mathbf{f}_*}$  are the mean vectors at the pseudo-points and prediction points respectively. For observation model

$$p(\mathbf{y} | \mathbf{f}) = \mathcal{N}(\mathbf{y}; \mathbf{f}, \mathbf{S}) \quad (5)$$

where  $\mathbf{S} \in \mathbb{R}^{N \times N}$  is a positive-definite diagonal matrix, it is possible to find the optimal  $q(\mathbf{u})$  in closed-form:

$$q(\mathbf{u}) \propto \mathcal{N}(\mathbf{y}; \mathbf{C}_{\mathbf{f} \mathbf{u}} \Lambda_{\mathbf{u}} \mathbf{u}, \mathbf{S}) \mathcal{N}(\mathbf{u}; \mathbf{0}, \mathbf{C}_{\mathbf{u}}) \quad (6)$$

and the ELBO at this optimum is also closed-form:

$$\mathcal{L} = \log \mathcal{N}(\mathbf{y}; \mathbf{m}_{\mathbf{f}}, \mathbf{C}_{\mathbf{f} \mathbf{u}} \Lambda_{\mathbf{u}} \mathbf{C}_{\mathbf{u} \mathbf{f}} + \mathbf{S}) - \frac{1}{2} \text{tr}(\mathbf{S}^{-1}(\mathbf{C}_{\mathbf{f}} - \mathbf{C}_{\mathbf{f} \mathbf{u}} \Lambda_{\mathbf{u}} \mathbf{C}_{\mathbf{u} \mathbf{f}})), \quad (7)$$

and is known as the *saturated bound*. It can be computed using only  $\mathcal{O}(NM^2)$  operations using the matrix inversion and determinant lemmas

**Related Models** The optimal  $q(\mathbf{u})$  coincides with the exact posterior distribution over  $\mathbf{u}$  under an *approximate model* with observation density  $\mathcal{N}(\mathbf{y}; \mathbf{C}_{\mathbf{f} \mathbf{u}} \Lambda_{\mathbf{u}} \mathbf{u}, \mathbf{S})$ , and that the first term in  $\mathcal{L}$  is the log marginal likelihood under this approximate model. It is well known that this is precisely the approximation employed by Seeger et al. [2003], known as the *Deterministic Training Conditional* (DTC). Despite their

similarities, the DTC log marginal likelihood and the ELBO typically yield quite different kernel parameters and pseudo-inputs when optimised for – while the pseudo-inputs  $\mathbf{z}_{1:M}$  are variational parameters in the variational approximation, and therefore not subject to overfitting (see section 2. of Bui et al. [2017]), they are model parameters in the DTC. For this reason, the variational approximation is widely favoured over the DTC.

However, this close relationship between the variational approximation and the DTC is utilised in Sec. 5 to obtain algorithms which combine pseudo-point and state-space approximations in a manner which is both efficient, and easy to implement.

**Benefits and Limitations** Pseudo-point approximations perform well when many more observations of a GP are made than are needed to accurately describe its posterior. This is often the case for regression tasks where the inputs are sampled independently. In this case the value of  $M$  required to maintain an accurate approximation as  $N$  increases generally seems not to grow too quickly—indeed Burt et al. [2019] showed that if the inputs  $\mathbf{x}_n$  are sampled i.i.d. from a Gaussian, then the value of  $M$  required scales roughly logarithmically in  $N$ . However, Bui and Turner [2014] noted that this is typically not the case for time series problems, where the interval in which the observations live typically grows linearly in  $N$ . Indeed Tobar [2019] showed that the number of the pseudo-points per unit time must not drop below a rate analogous to the Nyquist-Shannon rate if an accurate posterior approximation is to be maintained as  $N$  grows. Consequently the number of pseudo-points  $M$  required to maintain a good approximation must grow linearly in  $N$ , so the cost of accurate approximate inference using pseudo-point methods is really  $\mathcal{O}(N^3)$  in this case.

## 4 STATE SPACE APPROXIMATIONS TO SUM-SEPARABLE SPATIO-TEMPORAL GPs

Many time-series GPs can be augmented with additional latent dimensions in such a way that the marginal distribution over the original process is unchanged, but with the highly beneficial property that conditioning on all  $D$  dimensions at any point in time renders past and future time points independent [Särkkä and Solin, 2019]. This augmentation is exact for many GPs, in particular the popular half-integer Matérn family, and a good approximation for others, such as those with exponentiated-quadratic kernels. Consequently, for any collection of  $T$  points in time,  $\tau_1 < \tau_2 < \dots < \tau_T$ , the augmented GP forms a  $D$ -dimensional Gauss-Markov chain, whose transition dynamics are a function of the kernel of the GP. This means that standard algorithms (similar to Kalman filtering) can be utilised to perform inference under Gaussian likelihoods, thus achieving linear scaling in

$T$ . This technique can be extended to separable and sum-separable spatio-temporal GPs for rectilinear grids of inputs, the details of which are as follows.

**Separable GPs** Let  $\bar{f}$  be such an augmentation of  $f$  such that the distribution over  $\bar{f}(\tau, \mathbf{r}, 1)$  is approximately equal to that of  $f(\tau, \mathbf{r})$ , and conditioning on all latent dimensions renders  $\bar{f}$  Markov in  $\tau$ .  $\bar{f}$  is specified implicitly through a linear stochastic differential equation, meaning that inference under Gaussian observations can be performed efficiently via filtering / smoothing in a Linear-Gaussian State Space Model (LGSSM). Let  $\bar{\mathbf{f}}_t$  be the collection of random variables in  $\bar{f}$  at inputs given by the Cartesian product between the singleton  $\{t\}$ ,  $N_T$  arbitrary locations in space  $\mathbf{r}_{1:N_T}$ , and all of the latent dimensions  $\{1, \dots, D\}$ . Let the kernel of  $f$  be separable:  $\kappa((\mathbf{r}, \tau), (\mathbf{r}', \tau')) = \kappa^{\mathbf{r}}(\mathbf{r}, \mathbf{r}') \kappa^{\tau}(\tau, \tau')$ . Any collection of finite dimensional marginals  $\bar{\mathbf{f}} := \bar{\mathbf{f}}_{1:T}$ , each using the same  $\mathbf{r}_{1:N_T}$ , form an LGSSM with  $N_T D$ -dimensional state with dynamics

$$\bar{\mathbf{f}}_t \mid \bar{\mathbf{f}}_{t-1} \sim \mathcal{N}([\mathbf{I}_{N_T} \otimes \mathbf{A}_t] \bar{\mathbf{f}}_{t-1}, \mathbf{C}_f^{\mathbf{r}} \otimes \mathbf{Q}_t) \quad (8)$$

$$\mathbf{H}_{ab} := \mathbf{I}_a \otimes [\mathbf{1} \quad \mathbf{0}_{1 \times b-1}] \quad (9)$$

$$\bar{\mathbf{f}}_t = \mathbf{H}_{N_T D} \bar{\mathbf{f}}_t, \quad (10)$$

$$\mathbf{y}_t \mid \bar{\mathbf{f}}_t \sim \mathcal{N}(\bar{\mathbf{f}}_t, \mathbf{S}_t) \quad (11)$$

where  $\otimes$  denotes the Kronecker product,  $\mathbf{A}_t \in \mathbb{R}^{D \times D}$  and  $\mathbf{Q}_t \in \mathbb{R}^{D \times D}$  are functions of  $\kappa^{\tau}$ ,  $\mathbf{Q}_t$  is positive definite,  $\mathbf{C}_f^{\mathbf{r}}$  is the covariance matrix associated with  $\kappa^{\mathbf{r}}$  and  $\mathbf{r}_{1:N_T}$ ,  $\mathbf{0}_{p \times q}$  is a  $p \times q$  matrix of zeros,  $\mathbf{y}_t$  is the block of  $\mathbf{y}$  containing the observations at the  $t^{\text{th}}$  time, and the diagonal matrix  $\mathbf{S}_t$  is the on-diagonal block of  $\mathbf{S}$  corresponding to  $\mathbf{y}_t$ . See Solin [2016] for further details about  $\mathbf{A}_t$  and  $\mathbf{Q}_t$ .

**Sum-Separable GPs** Let  $f$  be the sum-separable GP given by summing over  $f_p \sim \mathcal{GP}(0, \kappa_p)$ . A state space approximation to  $f$  is obtained by constructing a  $D_p$ -dimensional state space approximation for each  $f_p$ , the finite dimensional marginals of which form an LGSSM

$$\bar{\mathbf{f}}_t^p \mid \bar{\mathbf{f}}_{t-1}^p \sim \mathcal{N}([\mathbf{I}_{N_T} \otimes \mathbf{A}_t^p] \bar{\mathbf{f}}_{t-1}^p, [\mathbf{C}_f^{\mathbf{r},p} \otimes \mathbf{Q}_t^p]) \quad (12)$$

$$\bar{\mathbf{f}}_t = \sum_{p=1}^P \mathbf{H}_{N_T D_p} \bar{\mathbf{f}}_t^p \quad (13)$$

where  $\mathbf{A}_t^p$ ,  $\mathbf{Q}_t^p$ , and  $\mathbf{C}_f^{\mathbf{r},p}$  are defined in the same way as above for each  $f_p$ , and  $\mathbf{y}_t \mid \bar{\mathbf{f}}_t$  is again given by Eq. (11). This LGSSM has  $N_T \sum_{p=1}^P D_p$  latent dimensions, increasing the time and memory needed to perform inference when compared to a separable model, and is the price of a more flexible model.

**Benefits and Limitations** While this formulation truly scales linearly in  $T$  it has two clear limitations, (i) all locations of observations must lie on a rectilinear time-space grid if any computational gains are to be achieved; and (ii) inference scales cubically in  $N_T$ , meaning that inference is

rendered infeasible by time or memory constraints if a large number of spatial locations are observed.

## 5 EXPLOITING SEPARABILITY TO OBTAIN THE BEST OF BOTH WORLDS

We now turn to the main contribution of this work: combining the pseudo-point and state space approximations. The result is an approximation which is applicable to any sum-separable GP whose time kernels can be approximated by a linear SDE. We do this simply by constructing a variational pseudo-point approximation of the state space approximation to the original process. In cases where the state space approximation is exact, this is similar to constructing an inter-domain pseudo-point approximation [Lazaro-Gredilla and Figueiras-Vidal, 2009] to the original process, where some of the pseudo-points are placed in auxiliary dimensions.

In this section we show that by constraining the pseudo-inputs, approximate inference becomes linear in time.

### 5.1 THE CONDITIONAL INDEPENDENCE STRUCTURE OF SEPARABLE GPS

O’Hagan [1998] showed that a separable GP  $f(\mathbf{r}, \tau)$  has the following conditional independence properties:

$$f(\mathbf{r}, \tau) \perp\!\!\!\perp f(\mathbf{r}', \tau') \mid f(\mathbf{r}, \tau'), \quad (14)$$

$$f(\mathbf{r}, \tau) \perp\!\!\!\perp f(\mathbf{r}', \tau') \mid f(\mathbf{r}', \tau). \quad (15)$$

These are explained graphically in Fig. 2. It is straightforward to show (see App. A.1) that this property extends to

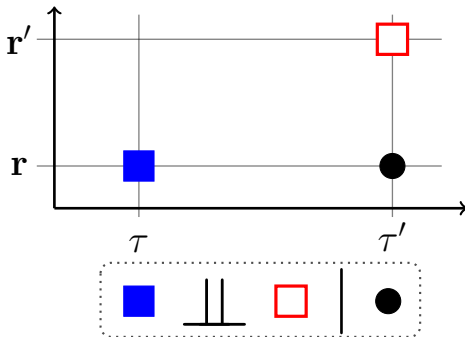


Figure 2: Depiction of the conditional independence property in Eq. (14). The blue square is  $f(\mathbf{r}, \tau)$ , the red square is  $f(\mathbf{r}', \tau')$ , and the black circle is  $f(\mathbf{r}, \tau')$ .

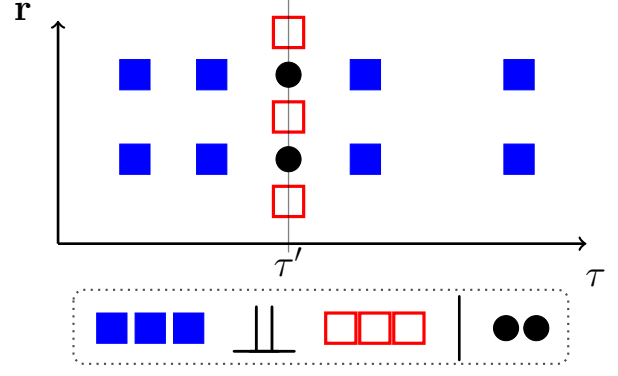


Figure 3: Depiction of the conditional independence property in Eq. (16). The blue squares are  $f(\mathcal{R}, \mathcal{T})$ , the red squares are  $f(\mathcal{R}', \mathcal{T}')$ , and the black circles are  $f(\mathcal{R}, \mathcal{T}')$ .

collections of random variables in  $f$ :

$$f(\mathcal{R}, \mathcal{T}) \perp\!\!\!\perp f(\mathcal{R}', \mathcal{T}') \mid f(\mathcal{R}, \mathcal{T}') \quad \text{where} \quad (16)$$

$$f(\mathcal{R}, \mathcal{T}) := \{f(\mathbf{r}, \tau) \mid \mathbf{r} \in \mathcal{R}, \tau \in \mathcal{T}\}$$

$$f(\mathcal{R}', \mathcal{T}') := \{f(\mathbf{r}, \tau') \mid \mathbf{r} \in \mathcal{R}'\}$$

$$f(\mathcal{R}, \mathcal{T}') := \{f(\mathbf{r}, \tau') \mid \mathbf{r} \in \mathcal{R}\}$$

where  $\mathcal{R}$  and  $\mathcal{R}'$  are sets of points in space,  $\mathcal{T}$  is a set of points through time, and  $\tau' \in \mathcal{T}$ . This conditional independence property is depicted in Fig. 3, and it is this second property that sits at the core of the approximation introduced in the next section.

### 5.2 COMBINING THE APPROXIMATIONS

We now combine the pseudo-point and state space approximations, and show how a temporal conditional independence property means that the optimal approximate posterior is Markov. This in turn leads to a closed-form expression for the optimum under Gaussian observation models and the existence of a simplified LGSSM in which exact inference yields optimal approximate inference in the original model.

**Pseudo-Point Approximation of State Space Augmentation** We perform approximate inference in a separable GP  $f$  with the kernel in Eq. (1) by applying the standard variational pseudo-point approximation (Sec. 3) to its state space augmentation (Sec. 4)  $\tilde{f}$ :

$$q(\tilde{f}) := q(\tilde{\mathbf{u}}) p(\tilde{f}_{\neq \tilde{\mathbf{u}}} \mid \tilde{\mathbf{u}}), \quad q(\tilde{\mathbf{u}}) = \mathcal{N}(\tilde{\mathbf{u}}; \mathbf{m}_{\tilde{\mathbf{u}}}^q, \mathbf{C}_{\tilde{\mathbf{u}}}^q),$$

where the pseudo-points  $\tilde{\mathbf{u}} = \tilde{\mathbf{u}}_{1:T}$  form a rectilinear grid of points in time, space, and *all* of the latent dimensions with the same structure as  $\mathbf{f}$  in Sec. 4, but replacing  $\mathbf{r}_{1:N_T}$  with a collection of  $M_\tau$  spatial pseudo-inputs,  $\mathbf{z}_{1:M_\tau}$ , for a total of  $TM_\tau D$  pseudo-points.  $p(\tilde{\mathbf{u}})$  is therefore Markov-through-time with conditional distributions

$$\tilde{\mathbf{u}}_t \mid \tilde{\mathbf{u}}_{t-1} \sim \mathcal{N}([\mathbf{I}_{M_\tau} \otimes \mathbf{A}_t] \tilde{\mathbf{u}}_{t-1}, \mathbf{C}_{\tilde{\mathbf{u}}}^r \otimes \mathbf{Q}_t), \quad (17)$$

$$\mathbf{u}_t := \mathbf{H}_{M_\tau D} \tilde{\mathbf{u}}_t. \quad (18)$$

where  $\mathbf{C}_{\bar{\mathbf{u}}}^r$  is the covariance matrix associated with  $\kappa^r$  and  $\mathbf{z}_{1:M_\tau}$ . Note the resemblance to Eq. (8). No constraint is placed on the location of the pseudo-points in space, only that they must remain at the same place for all time points.

Crucially, we now relax the assumption that the inputs associated with  $\mathbf{f}$  must form a rectilinear grid. Instead, it is necessary only to require that each observation is made at one of the  $T$  times at which we have placed pseudo-points. We denote the number of observations at time  $t$  by  $N_t$ , and continue to denote by  $\mathbf{f}_t$  the set of observations at time  $t$ .

**Exploiting Conditional Independence** Due to O’Hagan [1998]’s conditional independence property,  $p(\bar{\mathbf{f}}_t | \bar{\mathbf{u}}) = p(\bar{\mathbf{f}}_t | \mathbf{u}_t)$ ; see App. A for details. Consequently, the reconstruction terms in the ELBO depend only on  $\mathbf{u}_t$  as opposed to the entirety of  $\bar{\mathbf{u}}$ :

$$\mathcal{L} = \sum_{t=1}^T r_t - \mathcal{KL}[q(\bar{\mathbf{u}}) \| p(\bar{\mathbf{u}})], \quad (19)$$

$$r_t := \mathbb{E}_{q(\mathbf{u}_t)} [\mathbb{E}_{p(\mathbf{f}_t | \mathbf{u}_t)} [\log p(\mathbf{y}_t | \mathbf{f}_t)]]$$

This property alone yields substantial computational savings – only the covariance between  $\mathbf{u}_t$  and  $\mathbf{f}_t$  need be computed, as opposed to all of  $\bar{\mathbf{u}}$  and  $\mathbf{f}_t$ . Moreover, this means that

$$\mathbf{C}_{\bar{\mathbf{u}}} \Lambda_{\bar{\mathbf{u}}} = \begin{bmatrix} \mathbf{B}_1 & & \mathbf{0} \\ & \ddots & \\ \mathbf{0} & & \mathbf{B}_T \end{bmatrix}, \quad \mathbf{B}_t := \mathbf{C}_{\mathbf{f}_t \mathbf{u}_t} \Lambda_{\mathbf{u}_t} \mathbf{H}_{M_\tau D}. \quad (20)$$

**The Optimal Approximate Posterior is Markov** As an immediate consequence of Eq. (19), and by the same argument as that made by Seeger [1999], highlighted by Oppé and Archambeau [2009], the optimal approximate posterior precision satisfies

$$\Lambda_{\bar{\mathbf{u}}}^q := \Lambda_{\bar{\mathbf{u}}} + \begin{bmatrix} \mathbf{G}_1 & & \mathbf{0} \\ & \ddots & \\ \mathbf{0} & & \mathbf{G}_T \end{bmatrix}, \quad \mathbf{G}_t := -2\nabla_{\mathbf{C}_t^q} r_t. \quad (21)$$

where  $\Lambda_{\bar{\mathbf{u}}}^q := [\mathbf{C}_{\bar{\mathbf{u}}}^q]^{-1}$ , and  $\mathbf{C}_t^q$  is the  $t^{th}$  block on the diagonal of  $\mathbf{C}_{\bar{\mathbf{u}}}^q$ . Recall that the precision matrix of a Gauss-Markov model is block tridiagonal (see e.g. Grigorievskiy et al. [2017]), so  $\Lambda_{\bar{\mathbf{u}}}$  is block tridiagonal. Further, the exact posterior precision of an LGSSM with a Gaussian observation model is given by the sum of this block tridiagonal precision matrix and a block-diagonal matrix with the same block size.  $\Lambda_{\bar{\mathbf{u}}}^q$  has precisely this form, so the optimal approximate posterior over  $\bar{\mathbf{u}}$  must be a Gauss-Markov chain.

**Approximate Inference via Exact Inference in an Approximate Model** The above is equivalent to the optimal approximate posterior having density proportional to

$$q(\bar{\mathbf{u}}) \propto \prod_{t=1}^T p(\bar{\mathbf{u}}_t | \bar{\mathbf{u}}_{t-1}) \mathcal{N}(\mathbf{y}_t^q; \bar{\mathbf{u}}_t, \mathbf{G}_t^{-1}), \quad (22)$$

where  $\mathbf{y}_1^q, \dots, \mathbf{y}_T^q$  are a collection of  $T$  surrogate observations, detailed in App. B.1. Thus the optimal  $q(\bar{\mathbf{u}})$  is given by exact inference in an LGSSM. Moreover, Ashman et al. [2020] (App. A) show that  $\mathbf{G}_t$  can be written as a sum of  $N_t$  rank-1 matrices.

**Solution for Gaussian Observation Models** Under a Gaussian observation model, the optimal approximate posterior is given by the exact posterior under the DTC observation model, as discussed in section Sec. 3. Eq. (20) means that the DTC observation model can be written as

$$\mathcal{N}(\mathbf{y}; \mathbf{C}_{\bar{\mathbf{u}}} \Lambda_{\bar{\mathbf{u}}} \bar{\mathbf{u}}, \mathbf{S}) = \prod_{t=1}^T \mathcal{N}(\mathbf{y}_t; \mathbf{B}_t \bar{\mathbf{u}}_t, \mathbf{S}_t). \quad (23)$$

In conjunction with  $p(\bar{\mathbf{u}})$ , this yields the required LGSSM.

This LGSSM can be exploited both to perform approximate inference and compute the saturated bound in linear time, repurposing existing code – see App. B.2. This LGSSM also makes it clear, for example, how to employ the parallelised inference procedures proposed by Särkkä and García-Fernández [2020] and Loper et al. [2020] within this approximation.

**Sum-Separable Models** Extending this approximation to sum-separable processes is similar to the standard state space approximation. The resulting LGSSM is

$$\begin{aligned} \bar{\mathbf{u}}_t^p | \bar{\mathbf{u}}_{t-1}^p &\sim \mathcal{N}([\mathbf{I}_{M_\tau} \otimes \mathbf{A}_t^p] \bar{\mathbf{u}}_{t-1}^p, [\mathbf{C}_{\bar{\mathbf{u}}}^{r,p} \otimes \mathbf{Q}_t^p]) \\ p(\mathbf{y}_t | \bar{\mathbf{u}}_t) &= \mathcal{N}(\mathbf{y}_t; \sum_{p=1}^P \mathbf{B}_t^p \bar{\mathbf{u}}_t^p, \mathbf{S}_t). \\ \mathbf{B}_t^p &:= \mathbf{C}_{\mathbf{f}_t^p \mathbf{u}_t^p} \Lambda_{\mathbf{u}_t^p} \mathbf{H}_{M_\tau D_p}. \end{aligned} \quad (24)$$

Note the resemblance to Eq. (12).

**Efficient Inference in the Conditionals** The structure present in each  $\mathbf{B}_t^p$  can be used to accelerate inference. In particular note that  $\mathbf{H}_{M_\tau D_p}$  has size  $M_\tau \times DM_\tau$  while  $\mathbf{C}_{\mathbf{f}_t^p \mathbf{u}_t^p}^p \Lambda_{\mathbf{u}_t^p}^p$  is  $N_t \times M_\tau$ . Certainly  $M_\tau \leq DM_\tau$  and typically  $M_\tau < N$ , so this linear transformation forms a bottleneck. App. F explores this property, and shows how to exploit it to accelerate inference.

**Computational Complexity** The total number of flops required to compute the saturated ELBO is  $T(DM_\tau)^3 + D^3 M_\tau^2 + M_\tau^2 \sum_{t=1}^T N_t$  to leading order. This is a great deal fewer when  $T$  is large than the  $M^3 + M^2 N = M_\tau^3 T^3 + M_\tau^2 T^2 N$  required if the bound is computed naively. Similar improvements are achieved when making posterior predictions.

**Utilising Other Pseudo-Point Approximations** The conditional independence property exploited to develop the variational approximation in this section also shines new light on the work of Hartikainen et al. [2011]. In the specific case of their equation 5, in which the observation model is (adopting their notation)  $p(\mathbf{y}_k | \mathbf{x}_k) =$

$\mathcal{N}(\mathbf{y}_k; [\mathbf{I}_N \otimes \mathbf{H}]\mathbf{x}_k, \mathbf{S}_t)$ , they perform approximate inference in  $p(\bar{\mathbf{u}})$  using the modified observation model

$$\tilde{p}(\mathbf{y}_t | \bar{\mathbf{u}}_t) := \mathcal{N}(\mathbf{y}_t; \mathbf{C}_{f_t \bar{\mathbf{u}}_t} \Lambda_{\bar{\mathbf{u}}_t} \bar{\mathbf{u}}_t, [\tilde{\mathbf{C}}_{\mathbf{y}}]_t),$$

$$[\tilde{\mathbf{C}}_{\mathbf{y}}]_t := \text{diag}(\mathbf{C}_{f_t} - \mathbf{C}_{f_t \bar{\mathbf{u}}_t} \Lambda_{\bar{\mathbf{u}}_t} \mathbf{C}_{\bar{\mathbf{u}}_t f_t}) + \mathbf{S}_t$$

which is inspired by the well-known FITC [Csat  and Oppel, 2002, Snelson and Ghahramani, 2005] approximation. However, due to O’Hagan [1998]’s conditional independence property, this is equivalent to

$$\tilde{p}(\mathbf{y} | \bar{\mathbf{u}}) := \mathcal{N}(\mathbf{y}; \mathbf{C}_{f \bar{\mathbf{u}}} \Lambda_{\bar{\mathbf{u}}} \bar{\mathbf{u}}, \tilde{\mathbf{C}}_{\mathbf{y}}),$$

$$\tilde{\mathbf{C}}_{\mathbf{y}} := \text{diag}(\mathbf{C}_f - \mathbf{C}_{f \bar{\mathbf{u}}} \Lambda_{\bar{\mathbf{u}}} \mathbf{C}_{\bar{\mathbf{u}} f}) + \mathbf{S}.$$

While Hartikainen et al. [2011] did not actually consider the Gaussian observation model in their work, it is clear from the above that they would have utilised *exactly* the FITC approximation applied to  $\tilde{f}$  had they done so.

Bui et al. [2017] showed that both FITC and VFE can be viewed as edge cases of the Power EP algorithm introduced by Minka [2004]. Consequently the equivalent approximate model generalised both that of FITC and VFE – only  $\tilde{\mathbf{C}}_{\mathbf{y}}$  is changed from FITC: let  $\alpha \in [0, 1]$ , then

$$\tilde{\mathbf{C}}_{\mathbf{y}} := \alpha \text{diag}(\mathbf{C}_f - \mathbf{C}_{f \bar{\mathbf{u}}} \Lambda_{\bar{\mathbf{u}}} \mathbf{C}_{\bar{\mathbf{u}} f}) + \mathbf{S}.$$

In short, most standard pseudo-point approximations can be straightforwardly combined with state space approximations for sum-separable spatio-temporal GPs in the manner that we propose due to the conditional independence property.

### Relationship with Other Approximation Techniques

There are several existing methods that could be used to scale GPs to large spatio-temporal problems beyond those already considered – each method makes different assumptions about the kinds of problems considered, therefore making different trade-offs relative to ours.

The popular Kronecker-product methods for separable kernels explored by Saat i [2012] are unable to handle heteroscedastic observation noise or missing data, scale cubically in time, and require observations to lie on a rectilinear grid. Our approach suffers none of these limitations.

Wilson and Nickisch [2015] introduced a pseudo-point approximation they call *Structured Kernel Interpolation* (SKI) which is closely-related to the Kronecker-product methods, but removes many of their constraints. In particular, SKI places pseudo-points on a grid across all input dimensions, and utilises them to construct a sparse approximation to the prior covariance matrix over the data – crucially it is local in the sense that the approximation to the covariance between the pseudo-points and any given point depends only on a handful of pseudo-points. SKI covers the domain in a regular grid of points, which results in exponential growth in

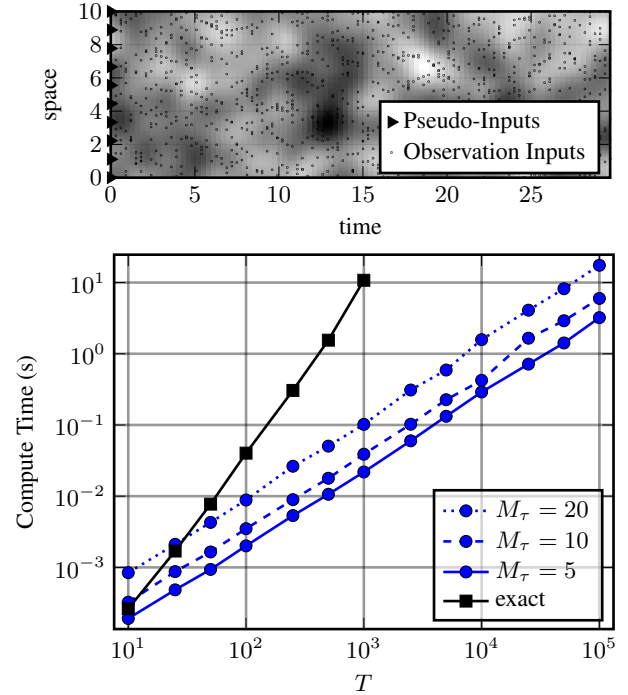


Figure 4: Arbitrary Spatial Locations. Top: Locations of (pseudo-)inputs for  $M_\tau = 10$ . 10 locations in space chosen randomly at each time point. Bottom: Time to compute ELBO vs performing exact inference. ELBO tight for  $M_\tau = 20$ ; see Fig. 11.

the number of pseudo-points as the number of dimensions grows. So, while this approximation scales very well in low-dimensional settings, it does not scale to input domains comprising more than a few dimensions. Moreover, to exploit this grid structure, separability across all dimensions is required. Gardner et al. [2018] alleviates this exponential scaling problem, but still require that the kernel be separable across all dimensions if their approximation is to be applied. Our approach does not suffer from this constraint as only the time dimension must be covered by pseudo-points – there are no constraints on their spatial locations. Naturally, that we do not perform similar approximations to SKI across the spatial dimensions means that our method will have the standard set of limitations experienced by all pseudo-point methods as the number of points in space grows. In short, the two classes of method are applicable to different kinds of spatio-temporal problems. They take somewhat orthogonal approaches to approximate inference, so combining them by utilising SKI across the spatial dimensions could offer the benefits of both classes of approximation in situations where SKI is applicable to the spatial component.

Similarly, approximations based on the relationship between GPs and Stochastic Partial Differential Equations [Whittle, 1963, Lindgren et al., 2011] could be combined with this work to improve scaling in space when the spatial kernel



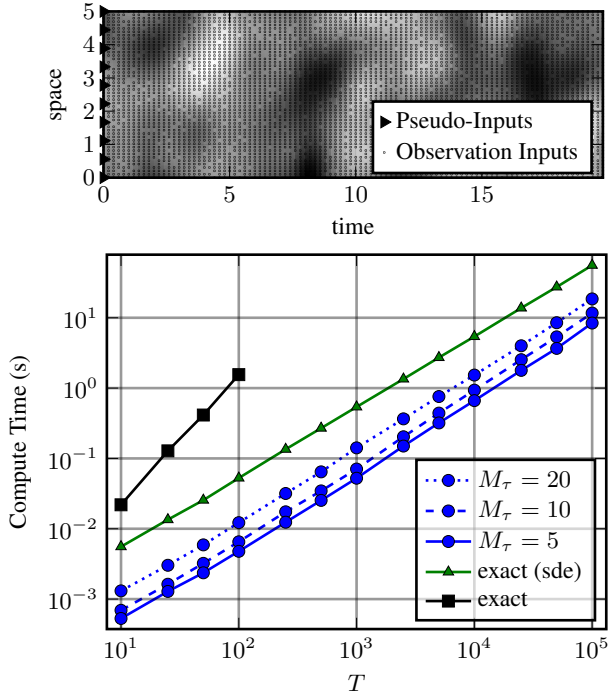


Figure 5: Grid-with-Missings. Top: Locations of (pseudo-)inputs – note the grid structure with 50 observations per time point, of which 5 are missing. Bottom: Time to compute ELBO vs LML naively and via state space methods (*sde*). ELBO tight for  $M_\tau = 20$ ; see Fig. 11.

is in the Matérn family. In low-dimensional settings other standard inter-domain pseudo-point approximations such as those of Hensman et al. [2017], Burt et al. [2020], and Dutordoir et al. [2020] could be applied.

## 6 EXPERIMENTS

We view the proposed approximation to be a useful contribution if it is able to outperform the vanilla state space approximation (Sec. 4), which is a strong baseline for the tasks we consider. To that end, we benchmark inference against synthetic data in Sec. 6.1, on a large-scale temperature modeling task to which both the vanilla and pseudo-point state space approximations can feasibly be applied (Sec. 6.2), and finally to a problem to which it is completely infeasible to apply the vanilla state space approximation (Sec. 6.3). We do not compare directly against the vanilla pseudo-point approximations of Titsias [2009] and Hensman et al. [2013]. As noted in Sec. 3, they are asymptotically no better than exact inference for problems with long time horizons.

### 6.1 BENCHMARKING

We first conduct two simple proof-of-concept experiments on synthetic data with a separable GP to verify our proposed method. In both experiments we consider quite a large tem-

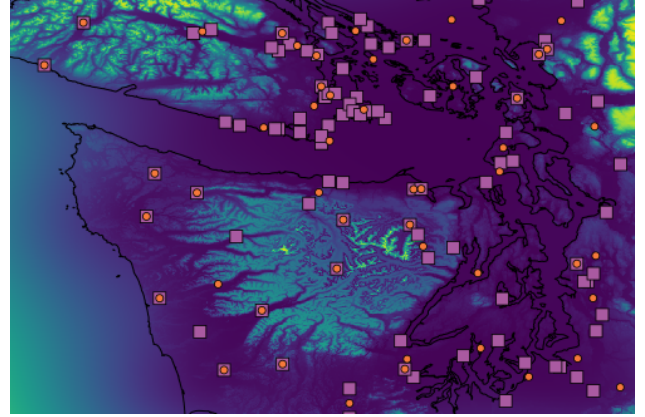


Figure 6: Posterior std. dev. counterpart to Fig. 1. The colour scale (0 to 1.75) is relative, pink squares are weather stations, and orange dots pseudo-points.

poral extent, but only moderate spatial, since we expect the proposed method to perform well in such situations – if the spatial extent of a data set is very large relative to the characteristic spatial variation, pseudo-point methods will struggle and, by extension, so will our method. App. E.1 contains additional details on the setup used, and App. E.1.1 contains the same experiments for a sum-separable model.

**Arbitrary Spatial Locations** Fig. 4 (top) shows how inputs were arranged for this experiment; at each time 10 spatial locations were sampled uniformly between 0 and 10, so  $N = 10T$ . The spatial location of pseudo-inputs are regular between 0 and 10. When using pseudo-points, we are indeed able to achieve substantial performance improvements relative to exact inference by utilising the state space methodology, while retaining a tight bound.

**Grid-with-Missings** Fig. 5 (top) shows how (pseudo) inputs were arranged for this experiment for  $M_\tau = 10$ ; the same 50 spatial locations are considered at each time point, but 5 of the observations are dropped at random, for a total of  $N_t = 45$  observations per time point – our largest case therefore involves  $N = 4.5 \times 10^6$  observations. The timing results show that we are able to compute a good approximation to the LML using roughly a third of the computation required by the standard state space approach to inference.

### 6.2 CLIMATOLOGY DATA

The Global Historical Climatology Network (GHCN) [Menne et al., 2012] comprises daily measurements of a variety of meteorological quantities, going back more than 100 years. We combine this data with the NASA Digital Elevation Model [NASA-JPL, 2020] to model the daily maximum temperature in the region  $(47^\circ, -127^\circ)$  and  $(49^\circ, -122^\circ)$ , which contains 99 weather stations. We utilise all data in this region since the year 2000, training on 90% (331522) and

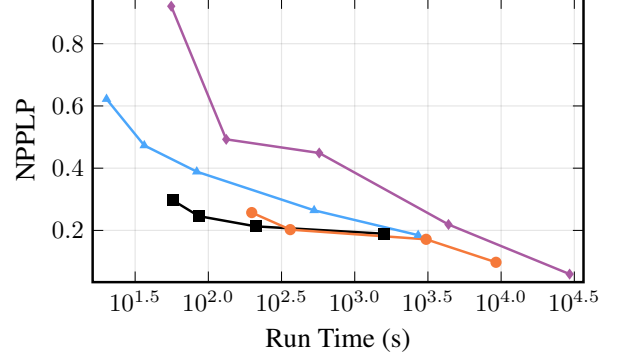
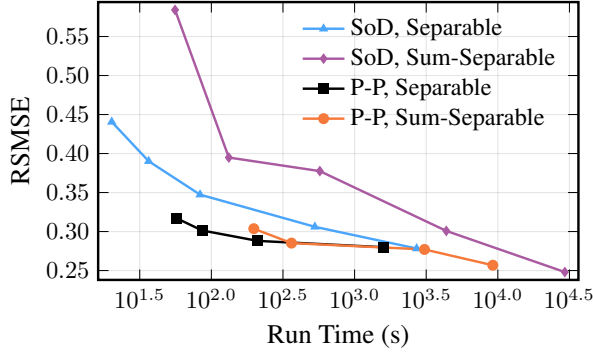


Figure 7: Test Root Standardised Mean-Squared Error (RSMSE) and Negative Posterior Predictive Log Probability (NPPLP). Marked points on Pseudo-Point curves used  $M \in \{5, 10, 20, 50\}$  moving from left to right – similarly for SoD markers, with the addition of  $M = 99$ , corresponding with the exact LML. Larger  $M$  improves performance, but time taken to train is increased. Sum-Separable models take longer to train than Separable but can produce better results.

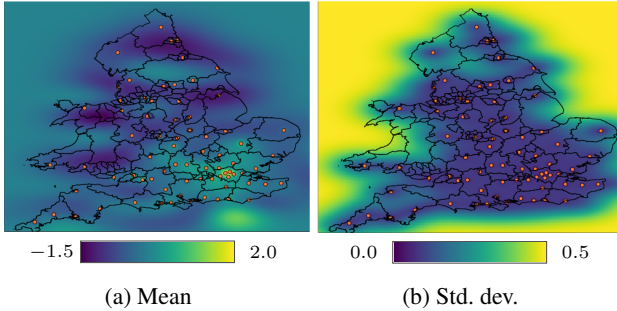


Figure 8: Apartment price posterior mean and standard deviation on a day near the end of 2020. Pseudo-point locations picked using K-means and marked with orange dots.

testing on 10% (36835) of the data. This experiment was conducted on a workstation with a 3.60 GHz Intel i7-7820X CPU (8 cores), and 46 GB of 3000 MHz DDR3 RAM.

Two models were utilised: a simple separable model with a Matérn- $\frac{5}{2}$  kernel over time, and Exponentiated Quadratic over space, and a sum of two such kernels with differing length scales and variances. Additional details in App. E.2.

Fig. 7 compares a simple subset-of-data (SoD) approximation, which is exact when  $M = 99$ , with the pseudo-point (P-P) approximation developed in this work. The results demonstrate that (i) the pseudo-point approximation has a more favourable speed-accuracy trade-off than the SoD, offering near exact inference in less time for a separable kernel, and (ii) a sum-separable model offers substantially improved results over a separable in this scenario.

### 6.3 APARTMENT PRICE DATA

Property sales data by postcode across England and Wales are provided by HM Land Registry [2014]. There are over  $10^6$  unique postcodes in England and Wales, of which a

Table 1: Performance on apartment price data.  $M_\tau = 75$ .

	RSMSE	NPPLP
Separable	0.658	2920
Sum-Separable	0.618	192

tiny proportion contain a sale on a given day. Consequently this data set has essentially arbitrary spatial locations at each point in time, which our approximation can handle, but which renders the vanilla state-space method infeasible.

We follow a similar procedure to Hensman et al. [2013], cross-referencing postcodes against a separate database [Camden, 2015] to obtain latitude-longitude coordinates, which we regress against the standardised logarithm of the price. However, we train on 843766 of the 1687536 apartment sales between 2010 and 2020, and test on the remainder. We again consider a separable and sum-separable GP that are similar to those in Sec. 6.2, but the temporal kernel is Matérn- $\frac{3}{2}$ . More detail in App. E.3.

Table 1 again demonstrates that a sum-separable model is able to capture more useful structure in the data than the separable model; Fig. 8 shows the variability and uncertainty in the prices on an arbitrarily chosen day.

## 7 DISCUSSION

This work shows that pseudo-point and state space approximations can be directly combined in the same model to effectively perform approximate inference and learning in sum-separable GPs, and ties up loose ends in the theory related to combining these models. This is important in spatio-temporal applications, where the model admits a form of an arbitrary-dimensional (spatial) random field with dynamics over a long temporal horizon. Experiments on synthetic and real-world data show that this approach enables a favourable



trade-off between computational complexity and accuracy.

Standard approximations for non-Gaussian observation models, such as those discussed by Wilkinson et al. [2020], Chang et al. [2020], and Ashman et al. [2020], can be applied straightforwardly within our approximation. Our method represents the simplest point in a range of possible approximations. As such there are several promising paths forward to achieve further scalability beyond simply utilising hardware acceleration, including (i) applying the estimator developed by Hensman et al. [2013] to our method to utilise mini batches of data, (ii) embedding the infinite-horizon approximation introduced by Solin et al. [2018] to trade off some accuracy for a substantial reduction in the computational complexity of our approximation, (iii) removing the constraint that observations must appear at the same time as pseudo-points by utilising the method developed by Adam et al. [2020].

**Code** [github.com/JuliaGaussianProcesses/TemporalGPs.jl](https://github.com/JuliaGaussianProcesses/TemporalGPs.jl) contains an implementation of the approximation developed in this work.

[github.com/willtebbutt/PseudoPointStateSpace-UAI-2021](https://github.com/willtebbutt/PseudoPointStateSpace-UAI-2021) contains code built on top of TemporalGPs.jl to reproduce the experiments.

### Author Contributions

WT conceived the idea, implemented models, and ran the experiments. All authors helped develop the idea, write the paper, and devise experiments.

### Acknowledgements

We thank Adrià Garriga-Alonso, Wessel Bruinsma, Matt Ashman, and anonymous reviewers for invaluable feedback. Will Tebbutt is supported by Deepmind and Invenia Labs. Arno Solin acknowledges funding from the Academy of Finland (grant id 324345). Richard E. Turner is supported by Google, Amazon, ARM, Improbable, Microsoft Research and EPSRC grants EP/M0269571 and EP/L000776/1.

### References

- Vincent Adam, Stefanos Eleftheriadis, Artem Artemev, Nicolas Durrande, and James Hensman. Doubly sparse variational Gaussian processes. In *International Conference on Artificial Intelligence and Statistics*, pages 2874–2884. PMLR, 2020.
- Matthew Ashman, Jonathan So, Will Tebbutt, Vincent Fortuin, Michael Pearce, and Richard E Turner. Sparse Gaussian process variational autoencoders. *arXiv preprint arXiv:2010.10177*, 2020.
- Thang D Bui and Richard E Turner. Tree-structured Gaussian process approximations. In *Advances in Neural Information Processing Systems 27*, pages 2213–2221. Curran Associates, Inc., 2014.
- Thang D Bui, Josiah Yan, and Richard E Turner. A unifying framework for Gaussian process pseudo-point approximations using power expectation propagation. *Journal of Machine Learning Research*, 18(1):3649–3720, 2017.
- David Burt, Carl Edward Rasmussen, and Mark van der Wilk. Rates of convergence for sparse variational Gaussian process regression. In *Proceedings of the 36th International Conference on Machine Learning*, volume 97 of *Proceedings of Machine Learning Research*, pages 862–871. PMLR, 2019.
- David R Burt, Carl Edward Rasmussen, and Mark van der Wilk. Variational orthogonal features. *arXiv preprint arXiv:2006.13170*, 2020.
- Open Data Camden. National Statistics Postcode Lookup UK Coordinates. <https://opendata.camden.gov.uk/Maps/National-Statistics-Postcode-Lookup-UK-Coordinates/77ra-mbbn>, 2015. [Online; accessed January-2021].
- Paul E Chang, William J Wilkinson, Mohammad Emtiyaz Khan, and Arno Solin. Fast variational learning in state-space Gaussian process models. In *2020 IEEE 30th International Workshop on Machine Learning for Signal Processing (MLSP)*, pages 1–6. IEEE, 2020.
- Jiahao Chen and Jarrett Revels. Robust benchmarking in noisy environments. *arXiv e-prints*, art. arXiv:1608.04295, Aug 2016.
- Lehel Csató and Manfred Opper. Sparse On-Line Gaussian Processes. *Neural computation*, 14(3):641–668, 2002.
- Vincent Dutoit, Nicolas Durrande, and James Hensman. Sparse gaussian processes with spherical harmonic features. In *International Conference on Machine Learning*, pages 2793–2802. PMLR, 2020.

- David Duvenaud, Hannes Nickisch, and Carl Edward Rasmussen. Additive Gaussian Processes. *Advances in Neural Information Processing Systems*, 24:226–234, 2011.
- Jacob Gardner, Geoff Pleiss, Ruihan Wu, Kilian Weinberger, and Andrew Wilson. Product Kernel Interpolation for Scalable Gaussian Processes. In *International Conference on Artificial Intelligence and Statistics*, pages 1407–1416. PMLR, 2018.
- Alexander Grigorievskiy, Neil Lawrence, and Simo Särkkä. Parallelizable sparse inverse formulation Gaussian processes (SpInGP). In *International Workshop on Machine Learning for Signal Processing (MLSP)*, pages 1–6. IEEE, 2017.
- Jouni Hartikainen, Jaakko Riihimäki, and Simo Särkkä. Sparse spatio-temporal Gaussian processes with general likelihoods. In *International Conference on Artificial Neural Networks*, pages 193–200. Springer, 2011.
- James Hensman, Nicolò Fusi, and Neil D. Lawrence. Gaussian processes for big data. In *Proceedings of the 29th Conference on Uncertainty in Artificial Intelligence (UAI)*, pages 282–290. AUAI Press, 2013.
- James Hensman, Alexander Matthews, and Zoubin Ghahramani. Scalable variational Gaussian process classification. In *Artificial Intelligence and Statistics*, pages 351–360, 2015.
- James Hensman, Nicolas Durrande, and Arno Solin. Variational fourier features for Gaussian processes. *The Journal of Machine Learning Research*, 18(1):5537–5588, 2017.
- HM Land Registry. Price Paid Data. <https://www.gov.uk/government/statistical-data-sets/price-paid-data-downloads>, 2014. [Online; accessed January-2021].
- Michael Innes. Don’t unroll adjoint: Differentiating ssa-form programs. *CoRR*, abs/1810.07951, 2018. URL <http://arxiv.org/abs/1810.07951>.
- Mohammad Khan and Wu Lin. Conjugate-computation variational inference: Converting variational inference in non-conjugate models to inferences in conjugate models. In *Artificial Intelligence and Statistics*, pages 878–887, 2017.
- Mohammad Emtiyaz Khan and Didrik Nielsen. Fast yet simple natural-gradient descent for variational inference in complex models. In *2018 International Symposium on Information Theory and Its Applications (ISITA)*, pages 31–35. IEEE, 2018.
- Miguel Lazaro-Gredilla and Anibal Figueiras-Vidal. Inter-domain Gaussian processes for sparse inference using inducing features. In *Advances in Neural Information Processing Systems*, pages 1087–1095, 2009.
- Finn Lindgren, Håvard Rue, and Johan Lindström. An Explicit Link Between Gaussian Fields and Gaussian Markov Random Fields: The Stochastic Partial Differential Equation Approach. *Journal of the Royal Statistical Society: Series B (Statistical Methodology)*, 73(4):423–498, 2011.
- Jackson Loper, David Blei, John P Cunningham, and Liam Paninski. General linear-time inference for Gaussian processes on one dimension. *arXiv preprint arXiv:2003.05554*, 2020.
- Alexander G. de G. Matthews, James Hensman, Richard E. Turner, and Zoubin Ghahramani. On sparse variational methods and the Kullback-Leibler divergence between stochastic processes. In *Proceedings of the 19th International Conference on Artificial Intelligence and Statistics*, volume 51 of *Proceedings of Machine Learning Research*, pages 231–239. PMLR, 2016.
- Matthew J Menne, Imke Durre, Russell S Vose, Byron E Gleason, and Tamara G Houston. An overview of the global historical climatology network-daily database. *Journal of Atmospheric and Oceanic Technology*, 29(7): 897–910, 2012.
- Thomas Minka. Power EP. Technical report, Technical report, Microsoft Research, Cambridge, 2004.
- Patrick Kofod Mogensen and Asbjørn Nilsen Riseth. Optim: A mathematical optimization package for Julia. *Journal of Open Source Software*, 3(24):615, 2018. doi: 10.21105/joss.00615.
- NASA-JPL. NASADEM Merged DEM Global 1 arc second V001 [Data set]. NASA EOSDIS Land Processes DAAC., 2020. URL [https://doi.org/10.5067/MEASUREs/NASADEM/NASADEM\\_HGT.001](https://doi.org/10.5067/MEASUREs/NASADEM/NASADEM_HGT.001).
- Manfred Opper and Cédric Archambeau. The variational Gaussian approximation revisited. *Neural Computation*, 21(3):786–792, 2009.
- Anthony O’Hagan. A Markov property for covariance structures. *Statistics Research Report*, 98:13, 1998.
- Joaquin Quiñero-Candela and Carl Edward Rasmussen. A unifying view of sparse approximate Gaussian process regression. *Journal of Machine Learning Research*, 6 (Dec):1939–1959, 2005.
- Carl Edward Rasmussen and Christopher KI Williams. *Gaussian Processes for Machine Learning*. The MIT Press, 2006.

- Yunus Saatçi. *Scalable Inference for Structured Gaussian Process Models*. PhD thesis, University of Cambridge, 2012.
- Simo Särkkä and Ángel F. García-Fernández. Temporal parallelization of Bayesian smoothers. *IEEE Transactions on Automatic Control*, 2020.
- Simo Särkkä and Arno Solin. *Applied Stochastic Differential Equations*. Cambridge University Press, 2019.
- Simo Särkkä, Arno Solin, and Jouni Hartikainen. Spatiotemporal learning via infinite-dimensional Bayesian filtering and smoothing: A look at Gaussian process regression through Kalman filtering. *IEEE Signal Processing Magazine*, 30(4):51–61, 2013.
- Matthias Seeger. Bayesian methods for support vector machines and gaussian processes. Technical report, University of Edinburgh, 1999.
- Matthias Seeger, Christopher Williams, and Neil Lawrence. Fast forward selection to speed up sparse Gaussian process regression. In *Proceedings of the Ninth International Workshop on Artificial Intelligence and Statistics*. Society for Artificial Intelligence and Statistics, 2003.
- Edward Snelson and Zoubin Ghahramani. Sparse Gaussian processes using pseudo-inputs. In *Advances in Neural Information Processing Systems*, pages 1257–1264. MIT Press, 2005.
- Arno Solin. *Stochastic differential equation methods for spatio-temporal Gaussian process regression*. PhD thesis, Aalto University, 2016.
- Arno Solin, James Hensman, and Richard E Turner. Infinite-horizon Gaussian processes. In *Proceedings of the 32nd International Conference on Neural Information Processing Systems*, pages 3490–3499, 2018.
- Michalis K Titsias. Variational learning of inducing variables in sparse Gaussian processes. In *Proceedings of the Twelfth International Conference on Artificial Intelligence and Statistics*, volume 5 of *Proceedings of Machine Learning Research*, pages 567–574. PMLR, 2009.
- Felipe Tobar. Band-limited Gaussian processes: The sinc kernel. In *Advances in Neural Information Processing Systems*, pages 12749–12759. Curran Associates, Inc., 2019.
- Peter Whittle. Stochastic-processes in several dimensions. *Bulletin of the International Statistical Institute*, 40(2): 974–994, 1963.
- William J Wilkinson, Paul E Chang, Michael Riis Andersen, and Arno Solin. State space expectation propagation: Efficient inference schemes for temporal Gaussian processes. In *Proceedings of the 32nd International Conference on Machine Learning (ICML)*, volume 119 of *Proceedings of Machine Learning Research*. PMLR, 2020.
- Andrew Wilson and Hannes Nickisch. Kernel interpolation for scalable structured Gaussian processes (KISS-GP). In *International Conference on Machine Learning*, pages 1775–1784, 2015.

---

## Supplementary Material: Combining Pseudo-Point and State Space Approximations for Sum-Separable Gaussian Processes

---

### A CONDITIONAL INDEPENDENCE RESULTS

#### A.1 THE CONDITIONAL INDEPENDENCE STRUCTURE OF COLLECTIONS OF POINTS

The following lemma establishes an analogue of the conditional independence result introduced by O’Hagan [1998], which applies to individual points, to collections of points in a separable Gaussian process.

**Lemma A.1.** *Let  $\mathcal{X}$  and  $\mathcal{Y}$  be sets,  $f \sim \mathcal{GP}(0, \kappa)$  where  $\kappa((x, y), (x', y')) := \kappa_x(x, x') \kappa_y(y, y')$ ,  $x, x' \in \mathcal{X}$  and  $y, y' \in \mathcal{Y}$ , and  $\kappa_x$  and  $\kappa_y$  are non-degenerate, meaning covariance matrices constructed using them are invertible. Then for finite sets  $\mathcal{X}_1, \mathcal{X}_2 \subset \mathcal{X}$ ,  $\mathcal{Y}_1, \mathcal{Y}_2 \subset \mathcal{Y}$ , and sets of random variables*

$$\begin{aligned} f(\mathcal{X}_1, \mathcal{Y}_1) &= \{f(x, y) \mid x \in \mathcal{X}_1, y \in \mathcal{Y}_1\}, \\ f(\mathcal{X}_2, \mathcal{Y}_2) &= \{f(x, y) \mid x \in \mathcal{X}_2, y \in \mathcal{Y}_2\}, \\ f(\mathcal{X}_2, \mathcal{Y}_1) &= \{f(x, y) \mid x \in \mathcal{X}_2, y \in \mathcal{Y}_1\}, \end{aligned}$$

it is the case that

$$f(\mathcal{X}_1, \mathcal{Y}_1) \perp\!\!\!\perp f(\mathcal{X}_2, \mathcal{Y}_2) \mid f(\mathcal{X}_2, \mathcal{Y}_1). \quad (25)$$

*Proof.* Since  $f(\mathcal{X}_1, \mathcal{Y}_1)$ ,  $f(\mathcal{X}_2, \mathcal{Y}_2)$ , and  $f(\mathcal{X}_2, \mathcal{Y}_1)$  are jointly Gaussian, it is sufficient to show that the conditional covariance  $\text{cov}(f(\mathcal{X}_1, \mathcal{Y}_1), f(\mathcal{X}_2, \mathcal{Y}_2) \mid f(\mathcal{X}_2, \mathcal{Y}_1))$  is always  $\mathbf{0}$ . Assign an arbitrary ordering to the elements in each of  $\mathcal{X}_1, \mathcal{X}_2, \mathcal{Y}_1$ , and  $\mathcal{Y}_2$ , and let  $\mathbf{C}_{\mathcal{X}_i \mathcal{X}_j}$  be the covariance matrix obtained by evaluating  $\kappa_x$  at each pair of points  $\mathcal{X}_i$  and  $\mathcal{X}_j$ , such that the  $(p, q)^{th}$  element of  $\mathbf{C}_{\mathcal{X}_i \mathcal{X}_j}$  is  $\kappa_x$  evaluated at the  $p^{th}$  and  $q^{th}$  elements of  $\mathcal{X}_i$  and  $\mathcal{X}_j$  respectively. Let  $\mathbf{C}_{\mathcal{Y}_i \mathcal{Y}_j}$  be analogously defined for  $\kappa_y$  and  $\mathcal{Y}_i, \mathcal{Y}_j$ . Denote the Kronecker product by  $\otimes$ , and order the elements of  $f(\mathcal{X}_1, \mathcal{Y}_1)$ ,  $f(\mathcal{X}_2, \mathcal{Y}_2)$ , and  $f(\mathcal{X}_2, \mathcal{Y}_1)$  such that

$$\begin{aligned} \text{cov}(f(\mathcal{X}_1, \mathcal{Y}_1), f(\mathcal{X}_2, \mathcal{Y}_2)) &= \mathbf{C}_{\mathcal{X}_1 \mathcal{X}_2} \otimes \mathbf{C}_{\mathcal{Y}_1 \mathcal{Y}_2}, \\ \text{cov}(f(\mathcal{X}_1, \mathcal{Y}_1), f(\mathcal{X}_2, \mathcal{Y}_1)) &= \mathbf{C}_{\mathcal{X}_1 \mathcal{X}_2} \otimes \mathbf{C}_{\mathcal{Y}_1 \mathcal{Y}_1}, \\ \text{cov}(f(\mathcal{X}_2, \mathcal{Y}_1), f(\mathcal{X}_2, \mathcal{Y}_2)) &= \mathbf{C}_{\mathcal{X}_2 \mathcal{X}_2} \otimes \mathbf{C}_{\mathcal{Y}_1 \mathcal{Y}_2}, \\ \text{cov}(f(\mathcal{X}_2, \mathcal{Y}_1)) &= \mathbf{C}_{\mathcal{X}_2 \mathcal{X}_2} \otimes \mathbf{C}_{\mathcal{Y}_1 \mathcal{Y}_1}. \end{aligned}$$

$\kappa_x$  and  $\kappa_y$  are non-degenerate, so  $\mathbf{C}_{\mathcal{X}_2 \mathcal{X}_2}$ ,  $\mathbf{C}_{\mathcal{Y}_1 \mathcal{Y}_1}$ , and  $\text{cov}(f(\mathcal{X}_2, \mathcal{Y}_1))$  are invertible, and the conditional covariance is

$$\begin{aligned} &\text{cov}(f(\mathcal{X}_1, \mathcal{Y}_1), f(\mathcal{X}_2, \mathcal{Y}_2) \mid f(\mathcal{X}_2, \mathcal{Y}_1)) \\ &= \text{cov}(f(\mathcal{X}_1, \mathcal{Y}_1), f(\mathcal{X}_2, \mathcal{Y}_2)) - \text{cov}(f(\mathcal{X}_1, \mathcal{Y}_1), f(\mathcal{X}_2, \mathcal{Y}_1)) \text{cov}(f(\mathcal{X}_2, \mathcal{Y}_1))^{-1} \text{cov}(f(\mathcal{X}_2, \mathcal{Y}_1), f(\mathcal{X}_2, \mathcal{Y}_2)) \\ &= \mathbf{C}_{\mathcal{X}_1 \mathcal{X}_2} \otimes \mathbf{C}_{\mathcal{Y}_1 \mathcal{Y}_2} - (\mathbf{C}_{\mathcal{X}_1 \mathcal{X}_2} \otimes \mathbf{C}_{\mathcal{Y}_1 \mathcal{Y}_1}) (\mathbf{C}_{\mathcal{X}_2 \mathcal{X}_2} \otimes \mathbf{C}_{\mathcal{Y}_1 \mathcal{Y}_1})^{-1} (\mathbf{C}_{\mathcal{X}_2 \mathcal{X}_2} \otimes \mathbf{C}_{\mathcal{Y}_1 \mathcal{Y}_2}) \\ &= \mathbf{C}_{\mathcal{X}_1 \mathcal{X}_2} \otimes \mathbf{C}_{\mathcal{Y}_1 \mathcal{Y}_2} - (\mathbf{C}_{\mathcal{X}_1 \mathcal{X}_2} \mathbf{C}_{\mathcal{X}_2 \mathcal{X}_2}^{-1} \mathbf{C}_{\mathcal{X}_2 \mathcal{X}_2}) (\mathbf{C}_{\mathcal{Y}_1 \mathcal{Y}_1} \mathbf{C}_{\mathcal{Y}_1 \mathcal{Y}_1}^{-1} \mathbf{C}_{\mathcal{Y}_1 \mathcal{Y}_2}) \\ &= \mathbf{C}_{\mathcal{X}_1 \mathcal{X}_2} \otimes \mathbf{C}_{\mathcal{Y}_1 \mathcal{Y}_2} - \mathbf{C}_{\mathcal{X}_1 \mathcal{X}_2} \otimes \mathbf{C}_{\mathcal{Y}_1 \mathcal{Y}_2} \\ &= \mathbf{0}. \end{aligned} \quad \square$$

This result is depicted in Fig. 9 – specifically letting  $f(\mathcal{X}_1, \mathcal{Y}_1)$  be the red squares,  $f(\mathcal{X}_2, \mathcal{Y}_2)$  the blue squares, and  $f(\mathcal{X}_2, \mathcal{Y}_1)$  the black dots.  $\mathcal{X}_1$  are the  $x$ -coordinates of the red squares,  $\mathcal{X}_2$  the  $x$ -coordinates of the blue squares / black circles,  $\mathcal{Y}_1$  the  $y$ -coordinates of the red squares / black circles, and  $\mathcal{Y}_2$  the  $y$ -coordinates of the blue squares.

Lemma A.1 establishes that a GP being separable implies the presented conditional independence between collections of points. O’Hagan [1998] goes further in the single-point case, also showing that the conditional independence property implies separability, hence showing that the separability and conditional independence statements are equivalent. While it seems plausible that such an equivalence could be established for collections of points, such a result is not needed in this work, and is therefore not pursued.

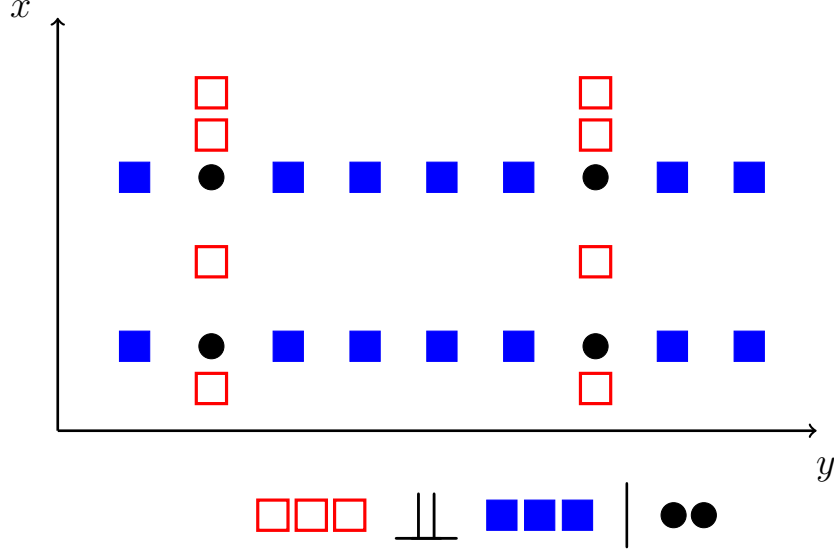


Figure 9: Under a separable GP prior, the random variables at the red squares are conditionally independent of those at the blue squares given those at the black circles.

## A.2 SEPARABILITY OF THE STATE-SPACE APPROXIMATION

Solin [2016] shows in chapter 5 that a separable spatio-temporal GP  $f$ , whose time-kernel has Markov structure, can be expressed as another GP  $\bar{f}$  with some auxiliary dimensions. The kernel of  $\bar{f}$  is not given explicitly – instead it is expressed in terms of an infinite-dimensional Kalman filter. Consequently, it is unclear without further investigation whether or not the kernel over  $\bar{f}$  is separable. We show that, grouping together time and the latent dimension, it in fact separates over space and the grouped dimensions.

Let  $\tau \in \mathbb{R}$  denote a point in time, and samples from  $\bar{f}(\mathbf{r}, \tau, d)$  be the random variable in  $f$  associated with the spatial location  $\mathbf{r}$ , time point  $\tau$ , and latent dimension  $d$ . Denote  $\bar{f}_\tau = \bar{f}(\cdot, \tau, \cdot)$ , then Solin [2016] shows that

$$\bar{f}_\tau \sim \mathcal{GP}(0, \kappa_\tau(\mathbf{r}, \mathbf{r}') \alpha_\tau(d, d')) \quad (26)$$

and, for any  $\tau'$ , kernel  $\alpha_\tau : \{1, \dots, D\} \times \{1, \dots, D\} \rightarrow \mathbb{R}$  (isomorphic to a  $D \times D$  matrix), kernel over space  $\kappa_\tau$ . Let  $\mathcal{A}_{\tau \rightarrow \tau'} : \mathcal{X} \times \{1, \dots, D\} \rightarrow \mathcal{X} \times \{1, \dots, D\}$  be the linear transition operator,

$$\bar{f}_{\tau'} = \mathcal{A}_{\tau \rightarrow \tau'} \bar{f}_\tau + q_{\tau \rightarrow \tau'} \quad (27)$$

$$(\mathcal{A}_{\tau \rightarrow \tau'} \bar{f}_\tau)(\mathbf{r}, d) = \sum_{j=1}^D [\mathbf{A}_{\tau \rightarrow \tau'}]_{dj} \bar{f}_\tau(\mathbf{r}, j), \quad (28)$$

where each  $q_{\tau \rightarrow \tau'}$  is an independent GP, samples from which are functions  $\mathcal{X} \times \{1, \dots, D\} \rightarrow \mathbb{R}$ , and  $\mathbf{A}_{\tau \rightarrow \tau'}$  is a  $D \times D$  matrix of real numbers.

**Lemma A.2.** *Let  $\bar{f} \sim \mathcal{GP}(0, \bar{\kappa})$ , the distribution over any time-marginal  $\bar{f}_\tau$  be defined according to Eq. (26), and the conditional distribution over  $\bar{f}_{\tau'}$  given  $\bar{f}_\tau$  Eq. (27). It follows that  $\bar{\kappa}$  is separable, and of the form*

$$\bar{\kappa}((\mathbf{r}, \tau, d), (\mathbf{r}', \tau', d')) = \kappa_\tau(\mathbf{r}, \mathbf{r}') \kappa_{\tau d}((\tau, d), (\tau', d')) \quad (29)$$

for some kernel  $\kappa_{\tau d}$ .



*Proof.*

$$\begin{aligned}
\bar{\kappa}((\mathbf{r}, \tau, d), (\mathbf{r}', \tau', d')) &:= \text{cov}(\bar{f}(\mathbf{r}, \tau, d), \bar{f}(\mathbf{r}', \tau', d')) \\
&= \text{cov}(\bar{f}_\tau(\mathbf{r}, d), \bar{f}_{\tau'}(\mathbf{r}', d')) \\
&= \mathbb{E}[\bar{f}_\tau(\mathbf{r}, d) \bar{f}_{\tau'}(\mathbf{r}', d')] \\
&= \mathbb{E}[\bar{f}_\tau(\mathbf{r}, d) \{(\mathcal{A}_{\tau \rightarrow \tau'} \bar{f}_\tau)(\mathbf{r}', d') + q_{\tau \rightarrow \tau'}(\mathbf{r}', d')\}] \\
&= \mathbb{E}[\bar{f}_\tau(\mathbf{r}, d) \{(\mathcal{A}_{\tau \rightarrow \tau'} \bar{f}_\tau)(\mathbf{r}', d')\}].
\end{aligned}$$

where the penultimate equality follows from independence. Applying Eq. (28) yields

$$\begin{aligned}
\bar{\kappa}((\mathbf{r}, \tau, d), (\mathbf{r}', \tau', d')) &= \sum_{j=1}^D [\mathbf{A}_{\tau \rightarrow \tau'}]_{d'j} \mathbb{E}[\bar{f}_\tau(\mathbf{r}, d) \bar{f}_\tau(\mathbf{r}', j)] \\
&= \sum_{j=1}^D [\mathbf{A}_{\tau \rightarrow \tau'}]_{d'j} \mathbb{E}[\bar{f}(\mathbf{r}, \tau, d) \bar{f}(\mathbf{r}', \tau, j)]
\end{aligned}$$

Applying Eq. (26) yields

$$\begin{aligned}
\bar{\kappa}((\mathbf{r}, \tau, d), (\mathbf{r}', \tau', d')) &= \sum_{j=1}^D [\mathbf{A}_{\tau \rightarrow \tau'}]_{d'j} \kappa_{\mathbf{r}}(\mathbf{r}, \mathbf{r}') \alpha_\tau((d, j)) \\
&= \kappa_{\mathbf{r}}(\mathbf{r}, \mathbf{r}') \sum_{j=1}^D [\mathbf{A}_{\tau \rightarrow \tau'}]_{d'j} \alpha_\tau(d, j) \\
&= \kappa_{\mathbf{r}}(\mathbf{r}, \mathbf{r}') \kappa_{\tau d}((\tau, d), (\tau', d'))
\end{aligned}$$

where

$$\kappa_{\tau d}((\tau, d), (\tau', d')) := \sum_{j=1}^D [\mathbf{A}_{\tau \rightarrow \tau'}]_{d'j} \alpha_\tau(d, j).$$

□

### A.3 CONDITIONAL INDEPENDENCE STRUCTURE OF OBSERVATIONS AND PSEUDO-POINTS UNDER A SEPARABLE PRIOR

Assume that the set of pseudo-inputs  $\bar{\mathbf{z}}$  form the rectilinear grid

$$\bar{\mathbf{z}} := \mathcal{Z}_{\mathbf{r}} \times \mathcal{T} \times \{1, \dots, D\} \tag{30}$$

where  $\times$  denotes the Cartesian product, and  $\mathcal{Z}_{\mathbf{r}} \subset \mathcal{X}$  and  $\mathcal{T} \subset \mathbb{R}$  are the finite sets of spatial and temporal locations at which pseudo-inputs are present, with sizes  $M_\tau$  and  $T$  respectively. Let the pseudo-points be

$$\bar{\mathbf{u}} := \{\bar{f}(\mathbf{r}, \tau, d) \mid (\mathbf{r}, \tau, d) \in \bar{\mathbf{z}}\}. \tag{31}$$

Furthermore, let

$$\mathbf{u}_\tau := \{\bar{f}(\mathbf{r}, \tau, 1) \mid \mathbf{r} \in \mathcal{Z}_{\mathbf{r}}\}, \tag{32}$$

then  $\bar{\mathbf{u}} \setminus \mathbf{u}_\tau$  is the collection of all pseudo-points not in  $\mathbf{u}_\tau$ .

Let  $\mathcal{X}_1, \dots, \mathcal{X}_T \subset \mathcal{X}$  be finite sets of points in space, one for each point in  $\mathcal{T}$ . The set of points

$$\mathbf{x}_\tau := \{(\mathbf{r}, \tau, 1) \mid \mathbf{r} \in \mathcal{X}_\tau\} \tag{33}$$

are the elements of  $\bar{f}$  which are observed (noisily) at time  $\tau$ , so let

$$\mathbf{f}_\tau := \{\bar{f}(\mathbf{r}, \tau, d) \mid (\mathbf{r}, \tau, d) \in \mathbf{x}_\tau\} \tag{34}$$

It is now possible to present the key result:

**Theorem A.3.**

$$\mathbf{f}_\tau \perp\!\!\!\perp \bar{\mathbf{u}} \setminus \mathbf{u}_\tau \mid \mathbf{u}_\tau. \quad (35)$$

That is:  $\mathbf{f}_\tau$  is conditionally independent of all pseudo-points not in the first latent dimension of  $\bar{f}$  at time  $\tau$ , given all of the pseudo-points in the first latent dimension of  $\bar{f}$  at time  $\tau$  – Fig. 10 visualises this property.

*Proof.* Let  $\mathcal{X} := \mathcal{X}$  and  $\mathcal{Y} := \mathbb{R} \times \{1, \dots, D\}$  – i.e. group together time and latent dimension – and (abusing notation) let

$$\bar{f}(\mathbf{r}, (\tau, d)) := \bar{f}(\mathbf{r}, \tau, d), \quad \mathbf{r} \in \mathcal{X}, \quad (\tau, d) \in \mathcal{Y}. \quad (36)$$

By Lemma A.2 the kernel over  $\bar{f}$  is separable across  $\mathcal{X}$  and  $\mathcal{Y}$ . Applying Lemma A.1 to  $\bar{f}$  and

$$\mathcal{X}_1 := \mathcal{X}_\tau, \quad \mathcal{X}_2 := \mathcal{Z}_\tau, \quad \mathcal{Y}_1 := \{(\tau, 1)\}, \quad \text{and } \mathcal{Y}_2 := [\mathcal{T} \times \{1, \dots, D\}] \setminus \mathcal{Y}_1. \quad (37)$$

yields the desired result, as  $\bar{f}_{\mathcal{X}_1, \mathcal{Y}_1} = \mathbf{f}_\tau$ ,  $\bar{f}_{\mathcal{X}_2, \mathcal{Y}_2} = \bar{\mathbf{u}} \setminus \mathbf{u}_\tau$ , and  $\bar{f}_{\mathcal{X}_2, \mathcal{Y}_1} = \mathbf{u}_\tau$ .  $\square$

This result is depicted in Fig. 10. Of the entire 3 dimensional grid of pseudo-points, only those in the first latent dimension at the same time as  $\mathbf{f}_\tau$  are needed to achieve conditional independence from all others.

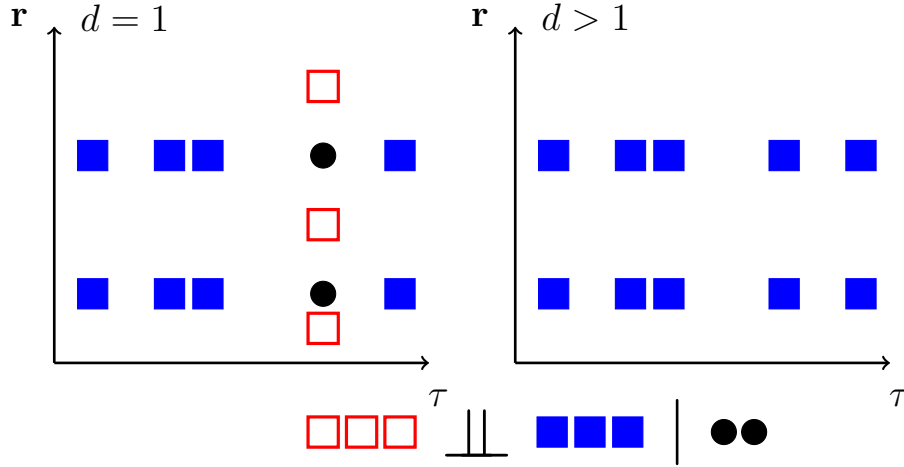


Figure 10: Slices of the 3-dimensional rectilinear grid of pseudo-points / inputs, as well as inputs of observations, depicting of the conditional independence structure presented in Theorem A.3. Unfilled red squares correspond to  $\mathbf{f}_\tau$ , black circles to  $\mathbf{u}_\tau$ , and filled blue squares to  $\bar{\mathbf{u}} \setminus \mathbf{u}_\tau$ . The left-hand side corresponds to  $d = 1$ , while the right-hand side corresponds to  $d > 1$ . Notice that  $\mathbf{u}_\tau$  and  $\mathbf{f}_\tau$  only appear in the  $d = 1$  slice.

#### A.4 CONDITIONAL INDEPENDENCE STRUCTURE UNDER A SUM-SEPARABLE PRIOR

Recall that a sum-separable GP  $\bar{f}^s$  is defined to be a GP of the form

$$\bar{f}^s := \sum_{p=1}^P \bar{f}^p, \quad \bar{f}^p \sim \mathcal{GP}(0, \bar{\kappa}^p), \quad (38)$$

where each  $\bar{f}^p$  is an independent separable GP. Locate rectilinear grids of pseudo-inputs in each of the separable processes:

$$\bar{\mathbf{z}}^p := \mathcal{Z}_\tau^p \times \mathcal{T} \times \{1, \dots, D\} \quad (39)$$

where  $\mathcal{Z}_\tau^p$  are a collection of points in space which are specific to each  $p$ . Each of these  $P$  grids of points is of the same form as those utilised for separable processes previously. Define sets of pseudo-points for each process:

$$\bar{\mathbf{u}}^p := \{\bar{f}^p(\mathbf{r}, \tau, d) \mid (\mathbf{r}, \tau, d) \in \bar{\mathbf{z}}^p\}, \quad (40)$$

$$\mathbf{u}_\tau^p := \{\bar{f}^p(\mathbf{r}, \tau, 1) \mid \mathbf{r} \in \mathcal{Z}_\tau^p\}, \quad (41)$$

$$p \in \{1, \dots, P\}, \quad (42)$$

and sets containing all of the of pseudo-points through the union of the above process-specific pseudo-points:

$$\bar{\mathbf{u}} := \bigcup_{p=1}^P \bar{\mathbf{u}}^p, \quad (43)$$

$$\mathbf{u}_\tau := \bigcup_{p=1}^P \mathbf{u}_\tau^p. \quad (44)$$

Furthermore, let

$$\mathbf{f}_\tau^p := \{\bar{f}^p(\mathbf{r}, \tau, 1) \mid \mathbf{r} \in \mathcal{X}_\tau\} \quad (45)$$

$$\mathbf{f}_\tau^s := \{\bar{f}^s(\mathbf{r}, \tau, 1) \mid \mathbf{r} \in \mathcal{X}_\tau\} \quad (46)$$

**Theorem A.4** (Conditional Independence in Sum-Separable GPs).

$$\mathbf{f}_\tau^s \perp\!\!\!\perp \bar{\mathbf{u}} \setminus \mathbf{u}_\tau \mid \mathbf{u}_\tau$$

*Proof.* As in Theorem A.3, it suffices to show that  $\text{cov}(\mathbf{f}_\tau^s, \bar{\mathbf{u}} \setminus \mathbf{u}_\tau \mid \mathbf{u}_\tau) = \mathbf{0}$ . It is the case that

$$\text{cov}(\bar{f}_s(\mathbf{r}, \tau, d), \bar{f}_p(\mathbf{r}', \tau', d')) = \text{cov}(\bar{f}_p(\mathbf{r}, \tau, d), \bar{f}_p(\mathbf{r}', \tau', d')), \quad (47)$$

and the covariance between any points in  $\bar{f}_p$  and  $\bar{f}_{p'}$  is 0 if  $p \neq p'$ , so

$$\begin{aligned} \text{cov}(\mathbf{f}_\tau^s, \bar{\mathbf{u}} \setminus \mathbf{u}_\tau) &= [\text{cov}(\mathbf{f}_\tau^1, \bar{\mathbf{u}}^1 \setminus \mathbf{u}_\tau^1) \quad \dots \quad \text{cov}(\mathbf{f}_\tau^P, \bar{\mathbf{u}}^P \setminus \mathbf{u}_\tau^P)] \\ \text{cov}(\mathbf{f}_\tau^s, \mathbf{u}_\tau) &= [\text{cov}(\mathbf{f}_\tau^1, \mathbf{u}_\tau^1) \quad \dots \quad \text{cov}(\mathbf{f}_\tau^P, \mathbf{u}_\tau^P)] \\ \text{cov}(\mathbf{u}_\tau) &= \begin{bmatrix} \text{cov}(\mathbf{u}_\tau^1) & & \mathbf{0} \\ & \ddots & \\ \mathbf{0} & & \text{cov}(\mathbf{u}_\tau^P) \end{bmatrix} \\ \text{cov}(\mathbf{u}_\tau, \bar{\mathbf{u}} \setminus \mathbf{u}_\tau) &= \begin{bmatrix} \text{cov}(\mathbf{u}_\tau^1, \bar{\mathbf{u}} \setminus \mathbf{u}_\tau^1) & & \mathbf{0} \\ & \ddots & \\ \mathbf{0} & & \text{cov}(\mathbf{u}_\tau^P, \bar{\mathbf{u}} \setminus \mathbf{u}_\tau^P) \end{bmatrix}. \end{aligned}$$

Therefore

$$\begin{aligned} \text{cov}(\mathbf{f}_\tau^s, \bar{\mathbf{u}} \setminus \mathbf{u}_\tau \mid \mathbf{u}_\tau) &= \text{cov}(\mathbf{f}_\tau^s, \bar{\mathbf{u}} \setminus \mathbf{u}_\tau) - \text{cov}(\mathbf{f}_\tau^s, \mathbf{u}_\tau) [\text{cov}(\mathbf{u}_\tau)]^{-1} \text{cov}(\mathbf{u}_\tau, \bar{\mathbf{u}} \setminus \mathbf{u}_\tau) \\ &= [\text{cov}(\mathbf{f}_\tau^1, \bar{\mathbf{u}}^1 \setminus \mathbf{u}_\tau^1 \mid \mathbf{u}_\tau^1) \quad \dots \quad \text{cov}(\mathbf{f}_\tau^P, \bar{\mathbf{u}}^P \setminus \mathbf{u}_\tau^P \mid \mathbf{u}_\tau^P)] \\ &= [\mathbf{0} \quad \dots \quad \mathbf{0}] \end{aligned} \quad (48)$$

where the final equality follows from Theorem A.3.  $\square$

## A.5 BLOCK-DIAGONAL STRUCTURE

Furthermore, this conditional independence property implies that

$$\mathbf{C}_{\mathbf{f}_t \bar{\mathbf{u}}} \mathbf{C}_{\bar{\mathbf{u}}}^{-1} = [\mathbf{0} \quad \dots \quad \mathbf{C}_{\bar{\mathbf{f}}_t \bar{\mathbf{u}}_t} \mathbf{C}_{\bar{\mathbf{u}}_t}^{-1} \quad \dots \quad \mathbf{0}]. \quad (49)$$

This is easily proven by considering that, were it not the case, then

$$\mathbb{E}[\mathbf{f}_t \mid \mathbf{u}] \neq \mathbb{E}[\mathbf{f}_t \mid \mathbf{u}_t], \quad (50)$$

for any non-zero  $\mathbf{u}$ , which is a contradiction. It follows from repeated application of Eq. (49) that the larger matrix  $\mathbf{C}_{\mathbf{f} \bar{\mathbf{u}}} \mathbf{C}_{\bar{\mathbf{u}}}^{-1}$  is block-diagonal, and is given by

$$\mathbf{C}_{\mathbf{f} \bar{\mathbf{u}}} \mathbf{C}_{\bar{\mathbf{u}}}^{-1} := \begin{bmatrix} \mathbf{C}_{\mathbf{f}_1 \bar{\mathbf{u}}} \mathbf{C}_{\bar{\mathbf{u}}}^{-1} \\ \vdots \\ \mathbf{C}_{\mathbf{f}_T \bar{\mathbf{u}}} \mathbf{C}_{\bar{\mathbf{u}}}^{-1} \end{bmatrix} = \begin{bmatrix} \mathbf{C}_{\mathbf{f}_1 \bar{\mathbf{u}}_1} \mathbf{C}_{\bar{\mathbf{u}}_1}^{-1} & & \mathbf{0} \\ & \ddots & \\ \mathbf{0} & & \mathbf{C}_{\mathbf{f}_T \bar{\mathbf{u}}_T} \mathbf{C}_{\bar{\mathbf{u}}_T}^{-1} \end{bmatrix}. \quad (51)$$

Similar manipulations reveal that the same property holds in the sum-separable case.

## B CONDITIONAL INDEPENDENCE PROPERTIES OF OPTIMAL APPROXIMATE OBSERVATION MODELS

Conditional independence structure in the observation model is reflected in the optimal approximate posterior, regardless the precise form of the observation model (Gaussian, Bernoulli, etc). Moreover, for Gaussian observation models, it is possible to find the model in which performing exact inference yields the optimal approximate posterior. These two properties are derived in the following two subsections.

### B.1 CONDITIONAL INDEPENDENCE STRUCTURE

This is only a slight extension of the result of Seeger [1999] and Opper and Archambeau [2009], which generalises from reconstruction terms which depend on only a one dimensional marginal of the Gaussian in question, to non-overlapping multi-dimensional marginals of arbitrary size. Let

$$p(\bar{\mathbf{u}}) := \mathcal{N}(\mathbf{u}; \mathbf{m}, \mathbf{C}), \quad q(\bar{\mathbf{u}}) := \mathcal{N}(\bar{\mathbf{u}}; \mathbf{m}^q, \mathbf{C}^q), \quad (52)$$

for  $\mathbf{m}, \mathbf{m}^q \in \mathbb{R}^N$  and positive-definite matrices  $\mathbf{C}, \mathbf{C}^q \in \mathbb{S}_+^N$ . Partition  $\bar{\mathbf{u}}$  into a collection of  $T$  sets,  $\bar{\mathbf{u}}_1, \dots, \bar{\mathbf{u}}_T$ , such that

$$\bar{\mathbf{u}} = \begin{bmatrix} \bar{\mathbf{u}}_1 \\ \vdots \\ \bar{\mathbf{u}}_T \end{bmatrix}. \quad (53)$$

Let  $\mathbf{m}_t$  and  $\mathbf{m}_t^q$  be the blocks of  $\mathbf{m}$  and  $\mathbf{m}^q$  corresponding to  $\bar{\mathbf{u}}_t$ . Similarly let  $\mathbf{C}_t$  and  $\mathbf{C}_t^q$  the on-diagonal blocks of  $\mathbf{C}$  and  $\mathbf{C}^q$  corresponding to  $\bar{\mathbf{u}}_t$ . Then the prior and approximate posterior marginals over  $\bar{\mathbf{u}}_t$  are

$$p(\bar{\mathbf{u}}_t) = \mathcal{N}(\bar{\mathbf{u}}_t; \mathbf{m}_t, \mathbf{C}_t), \quad q(\bar{\mathbf{u}}_t) = \mathcal{N}(\bar{\mathbf{u}}_t; \mathbf{m}_t^q, \mathbf{C}_t^q), \quad (54)$$

due to the marginalisation property of Gaussians.

Assume that the reconstruction term can be written as a sum over terms specific to each  $\bar{\mathbf{u}}_t$ ,

$$r(\mathbf{m}^q, \mathbf{C}^q) = \sum_{t=1}^T r_t(\mathbf{m}_t^q, \mathbf{C}_t^q), \quad (55)$$

for functions  $r_1, \dots, r_T$ . This is a useful assumption because it is satisfied for the model class considered in this work. Under this assumption, the optimal Gaussian approximate posterior density is proportional to

$$p(\bar{\mathbf{u}}) \prod_{t=1}^T \mathcal{N}(\mathbf{y}_t^q; \bar{\mathbf{u}}_t, [\mathbf{G}_t]^{-1}) \quad (56)$$

for appropriately-sized surrogate observations  $\mathbf{y}_1^q, \dots, \mathbf{y}_T^q$  and positive-definite precision matrices  $\mathbf{G}_1, \dots, \mathbf{G}_T$ , which is to say that the optimal approximate posterior is equivalent to the exact posterior under a “surrogate” Gaussian observation model whose density factorises across  $\bar{\mathbf{u}}_1, \dots, \bar{\mathbf{u}}_T$ .

A straightforward way to arrive at this result is via a standard result involving exponential families. Consider an exponential family prior

$$p(\bar{\mathbf{u}}) = h(\bar{\mathbf{u}}) \exp(\langle \eta, \phi(\bar{\mathbf{u}}) \rangle - A(\eta)), \quad (57)$$

where  $h$  is the base measure,  $\phi$  the sufficient-statistic function,  $A$  the log partition function, and  $\eta$  the natural parameters. and approximate posterior in the same family,

$$q(\bar{\mathbf{u}}) = h(\bar{\mathbf{u}}) \exp(\langle \eta^q, \phi(\bar{\mathbf{u}}) \rangle - A(\eta^q)), \quad (58)$$

which differs from  $p$  only in its natural parameters  $\eta^q$ . Let

$$p(\bar{\mathbf{u}} | \mathbf{y}) \propto p(\bar{\mathbf{u}}) p(\mathbf{y} | \bar{\mathbf{u}}) \quad (59)$$

be the posterior over  $\bar{\mathbf{u}}$  given observations  $\mathbf{y}$  under an arbitrary observation model  $p(\mathbf{y} | \bar{\mathbf{u}})$ . It is well-known (see e.g. Khan and Nielsen [2018]) that the  $\eta^q$  minimising  $\mathcal{KL}[q(\bar{\mathbf{u}}) \| p(\bar{\mathbf{u}} | \mathbf{y})]$  satisfies

$$\eta^q = \eta + (\nabla_{\mu} r)(\mu(\eta^q)). \quad (60)$$

where  $\mu$  denotes the expectation parameters  $\mu := \mathbb{E}_q[\phi(\bar{\mathbf{u}})]$  and, in an abuse of notation,  $\mu(\eta)$  denotes the function computing the mean parameter for any particular natural parameter. Given the canonical parameters  $\mathbf{m}$  and  $\mathbf{C}$  of a Gaussian, and letting  $\Lambda := [\mathbf{C}]^{-1}$ , its natural parameters and mean parameters are

$$\eta = (\eta_1, \eta_2) = (\Lambda \mathbf{m}, -\frac{1}{2} \Lambda), \quad \mu = (\mu_1, \mu_2) = (\mathbf{m}, \mathbf{m} \mathbf{m}^\top + \mathbf{C}). \quad (61)$$

Let  $\Lambda^q := [\mathbf{C}^q]^{-1}$  be the precision of  $q$ ,  $\Lambda := \mathbf{C}^{-1}$  the precision of  $p$ , and recall that the optimal Gaussian approximate posterior satisfies

$$\Lambda^q = \Lambda - 2 (\nabla_{\mathbf{C}^q} r)(\mathbf{m}^q, \mathbf{C}^q). \quad (62)$$

Due to the assumed structure in  $r$ ,  $\nabla_{\mathbf{C}^q} r$  is block-diagonal:

$$(\nabla_{\mathbf{C}^q} r)(\mathbf{m}^q, \mathbf{C}^q) = \begin{bmatrix} (\nabla_{\mathbf{C}_1^q} r_1)(\mathbf{m}_1^q, \mathbf{C}_1^q) & & \mathbf{0} \\ & \ddots & \\ \mathbf{0} & & (\nabla_{\mathbf{C}_T^q} r_T)(\mathbf{m}_T^q, \mathbf{C}_T^q) \end{bmatrix}. \quad (63)$$

Observe that each on-diagonal block involves only the corresponding term in  $r$ , i.e. the  $t^{th}$  block is only a function of  $r_t$ .

Equating the exact posterior precision under the approximate model in Eq. (56) with the optimal approximate posterior precision yields

$$\Lambda + \begin{bmatrix} \Lambda_1^q & & \mathbf{0} \\ & \ddots & \\ \mathbf{0} & & \Lambda_T^q \end{bmatrix} = \Lambda + \begin{bmatrix} -2 (\nabla_{\mathbf{C}_1^q} r_1)(\mathbf{m}_1^q, \mathbf{C}_1^q) & & \mathbf{0} \\ & \ddots & \\ \mathbf{0} & & -2 (\nabla_{\mathbf{C}_T^q} r_T)(\mathbf{m}_T^q, \mathbf{C}_T^q) \end{bmatrix} \quad (64)$$

From the above we deduce that letting  $\Lambda_t^q := -2 (\nabla_{\mathbf{C}_t^q} r_t)(\mathbf{m}_t^q, \mathbf{C}_t^q)$  ensures that the posterior precision under the surrogate model and the precision of the approximate posterior coincide for the optimal  $q$ .

Similarly, the optimal approximate posterior mean satisfies

$$\Lambda^q \mathbf{m}^q = \Lambda \mathbf{m} + [\nabla_{\mu} r]_1, \quad (65)$$

where  $[\nabla_{\mu} r]_1$  denotes the component of the gradient of  $r$  w.r.t.  $\mu$  corresponding to  $\mu_1$ . Equating the optimal posterior mean under the approximate model in Eq. (56) with that of the optimal approximate posterior yields

$$\begin{bmatrix} \mathbf{G}_1 & & \mathbf{0} \\ & \ddots & \\ \mathbf{0} & & \mathbf{G}_T \end{bmatrix} \begin{bmatrix} \mathbf{y}_1^q \\ \vdots \\ \mathbf{y}_T^q \end{bmatrix} = \begin{bmatrix} [\nabla_{\mu} r_1]_1 \\ \vdots \\ [\nabla_{\mu} r_T]_1 \end{bmatrix}. \quad (66)$$

This implies that  $\mathbf{y}_t^q := \mathbf{G}_t^{-1} [\nabla_{\mu} r]_{1t}$ .

## B.2 APPROXIMATE INFERENCE VIA EXACT INFERENCE

Recall the standard saturated bound introduced by Titsias [2009], that is obtained at the optimal approximate posterior:

$$\mathcal{L} = \log \mathcal{N}(\mathbf{y}; \mathbf{m}_f, \mathbf{C}_{f\bar{\mathbf{u}}} \Lambda_{\bar{\mathbf{u}}} \mathbf{C}_{\bar{\mathbf{u}}f} + \mathbf{S}) - \frac{1}{2} \text{tr}(\mathbf{S}^{-1} [\mathbf{C}_f - \mathbf{C}_{f\bar{\mathbf{u}}} \Lambda_{\bar{\mathbf{u}}} \mathbf{C}_{\bar{\mathbf{u}}f}]). \quad (67)$$

The first term is simply to log marginal likelihood of the LGSSM defined in Eq. (23) if  $f$  is separable, or Eq. (24) if it is sum-separable.



Recall from Eq. (20) that

$$\mathbf{C}_{\mathbf{f}\bar{\mathbf{u}}}\Lambda_{\bar{\mathbf{u}}} = \begin{bmatrix} \mathbf{B}_1 & & \mathbf{0} \\ & \ddots & \\ \mathbf{0} & & \mathbf{B}_T \end{bmatrix}, \quad (68)$$

$$\mathbf{B}_t := \mathbf{C}_{\mathbf{f}_t \mathbf{u}_t} \Lambda_{\mathbf{u}_t} \mathbf{H}_{M_\tau D},$$

so the trace term in Eq. (67) can be written as

$$\begin{aligned} \text{tr}(\mathbf{S}^{-1}[\mathbf{C}_{\mathbf{f}} - \mathbf{C}_{\mathbf{f},\bar{\mathbf{u}}}\Lambda_{\bar{\mathbf{u}}}\mathbf{C}_{\bar{\mathbf{u}},\mathbf{f}}]) &= \text{tr}(\mathbf{S}^{-1}[\mathbf{C}_{\mathbf{f}} - \mathbf{C}_{\mathbf{f},\bar{\mathbf{u}}}\Lambda_{\bar{\mathbf{u}}}\mathbf{C}_{\bar{\mathbf{u}}}\Lambda_{\bar{\mathbf{u}}}\mathbf{C}_{\bar{\mathbf{u}},\mathbf{f}}]) \\ &= \sum_{t=1}^T \text{tr}(\mathbf{S}_t^{-1}[\mathbf{C}_{\mathbf{f}_t} - \mathbf{B}_t \mathbf{C}_{\bar{\mathbf{u}}_t} \mathbf{B}_t]) \end{aligned} \quad (69)$$

$$\begin{aligned} &= \sum_{t=1}^T \text{tr}(\mathbf{S}_t^{-1}[\mathbf{C}_{\mathbf{f}_t} - \mathbf{C}_{\mathbf{f}_t \mathbf{u}_t} \Lambda_{\mathbf{u}_t} \mathbf{C}_{\mathbf{u}_t} \Lambda_{\mathbf{u}_t} \mathbf{C}_{\mathbf{u}_t \mathbf{f}_t}]) \\ &= \sum_{t=1}^T \text{tr}(\mathbf{S}_t^{-1}[\mathbf{C}_{\mathbf{f}_t} - \mathbf{C}_{\mathbf{f}_t \mathbf{u}_t} \Lambda_{\mathbf{u}_t} \mathbf{C}_{\mathbf{u}_t \mathbf{f}_t}]) \end{aligned} \quad (70)$$

These quantities can be computed either by running the approximate model forwards through time and computing the marginal statistics using Eq. (69), or via the  $\kappa^{\mathbf{r}}$  and  $\kappa^{\mathbf{r}}$  directly using Eq. (70).

Observe that, as with any  $\mathbf{f}_t$  from the training data, the marginal distribution over some  $\mathbf{f}_{*t}$  under the approximate posterior only involves  $\bar{\mathbf{u}}_t$  as  $\mathbf{f}_{*t} \perp\!\!\!\perp \bar{\mathbf{u}}_{\setminus t} \mid \bar{\mathbf{u}}_t$ :

$$\begin{aligned} q(\mathbf{f}_{*t}) &= \mathcal{N}(\mathbf{f}_{*t}; \hat{\mathbf{m}}_{\mathbf{f}_{*t}}, \mathbf{C}_{\mathbf{f}_{*t}}^{\mathbf{q}}) \text{ where} \\ \hat{\mathbf{m}}_{\mathbf{f}_{*t}} &:= \mathbf{m}_{\mathbf{f}_{*t}} + \mathbf{C}_{\mathbf{f}_{*t} \mathbf{u}_t} \Lambda_{\mathbf{u}_t} \mathbf{H}_{\mathbf{u}_t} (\hat{\mathbf{m}}_{\bar{\mathbf{u}}_t} - \mathbf{m}_{\bar{\mathbf{u}}_t}), \\ \mathbf{C}_{\mathbf{f}_{*t}}^{\mathbf{q}} &:= \mathbf{C}_{\mathbf{f}_{*t}} - \mathbf{C}_{\mathbf{f}_{*t} \mathbf{u}_t} \Lambda_{\mathbf{u}_t} \mathbf{H}_{\mathbf{u}_t} \left[ \mathbf{C}_{\bar{\mathbf{u}}_t} - [\hat{\Lambda}_{\bar{\mathbf{u}}_t}^*]^{-1} \right] \mathbf{H}_{\mathbf{u}_t}^{\top} \Lambda_{\mathbf{u}_t} \mathbf{C}_{\mathbf{u}_t \mathbf{f}_{*t}}. \end{aligned}$$

Performing smoothing in the approximate model provides  $\hat{\mathbf{m}}_{\bar{\mathbf{u}}_t}$  and  $[\hat{\Lambda}_{\bar{\mathbf{u}}_t}^*]^{-1}$ , from which the optimal approximate posterior marginals are straightforwardly obtained via the above.

## C FITC

Consider the approximate model employed by FITC:

$$\tilde{p}(\mathbf{y} \mid \bar{\mathbf{u}}) := \mathcal{N}(\mathbf{y}; \mathbf{m}_{\mathbf{f}} + \mathbf{C}_{\mathbf{f}\bar{\mathbf{u}}}\Lambda_{\bar{\mathbf{u}}}(\bar{\mathbf{u}} - \mathbf{m}_{\bar{\mathbf{u}}}), \text{diag}(\mathbf{C}_{\mathbf{f}} - \mathbf{C}_{\mathbf{f}\bar{\mathbf{u}}}\Lambda_{\bar{\mathbf{u}}}\mathbf{C}_{\bar{\mathbf{u}}\mathbf{f}}) + \mathbf{S}) \quad (71)$$

We know that in our separable setting,  $\mathbf{C}_{\mathbf{f}\bar{\mathbf{u}}}\Lambda_{\bar{\mathbf{u}}}$  is block-diagonal from App. A.5. This means that the  $t^{\text{th}}$  block on the diagonal of the conditional covariance matrix is

$$\mathbf{C}_{\mathbf{f}_t} - \mathbf{C}_{\mathbf{f}_t \bar{\mathbf{u}}_t} \Lambda_{\bar{\mathbf{u}}_t} \mathbf{C}_{\bar{\mathbf{u}}_t \mathbf{f}_t}, \quad (72)$$

and the entire conditional distribution factorises as follows:

$$\tilde{p}(\mathbf{y} \mid \bar{\mathbf{u}}) = \prod_{t=1}^T \mathcal{N}(\mathbf{y}_t; \mathbf{m}_{\mathbf{f}_t} + \mathbf{C}_{\mathbf{f}_t \bar{\mathbf{u}}_t} \Lambda_{\bar{\mathbf{u}}_t} (\bar{\mathbf{u}}_t - \mathbf{m}_{\bar{\mathbf{u}}_t}), \text{diag}(\mathbf{C}_{\mathbf{f}_t} - \mathbf{C}_{\mathbf{f}_t \bar{\mathbf{u}}_t} \Lambda_{\bar{\mathbf{u}}_t} \mathbf{C}_{\bar{\mathbf{u}}_t \mathbf{f}_t}) + \mathbf{S}_t). \quad (73)$$

By comparing this with equation 5 of [Hartikainen et al., 2011], and letting the observation model in that equation  $p(\mathbf{y}_k \mid \mathbf{x}_k) = \mathcal{N}(\mathbf{y}_k; [\mathbf{I}_N \otimes \mathbf{H}]\mathbf{x}_k, \mathbf{S}_t)$ , the correspondence is clear.

## D INFERENCE UNDER NON-GAUSSIAN OBSERVATION MODELS

While the optimal approximate posterior over the pseudo-points is not Gaussian, in line with most other approximations (e.g. [Hensman et al., 2015]) we restrict it to be so. As we have shown that the optimal approximate posterior precision is

block-tridiagonal regardless the observation model, it follows that the optimal Gaussian approximation must be a Gauss-Markov model. While in general such a model has a total of  $T(DM_\tau + 2(DM_\tau)^2)$  free (variational) parameters, in our case we know that the off-diagonal blocks of the precision are the same as in the prior, meaning that there are at most  $T(DM_\tau + (DM_\tau)^2)$  free (variational) parameters – this is also clear from Eq. (21). While one could directly parametrise the precision, this might be inconvenient from the perspective of numerical stability and implementation (standard filtering / smoothing algorithms do not work directly with the precision). Consequently, it probably makes sense to set up a surrogate model in line with that discussed by Khan and Lin [2017], Chang et al. [2020], and Ashman et al. [2020]. Alternatively one could parametrise the filtering distributions directly, from which the posterior marginals could be obtained using standard smoothing algorithms.

## E ADDITIONAL EXPERIMENT DETAILS

### E.1 BENCHMARKING EXPERIMENT

The kernel of the GP used in all experiments is

$$\kappa((\mathbf{r}, \tau), (\mathbf{r}', \tau')) = \kappa^{\mathbf{r}}(\mathbf{r}, \mathbf{r}') \kappa^{\tau}(\tau, \tau') \quad (74)$$

where  $\kappa^{\mathbf{r}}$  is an Exponentiated Quadratic kernel with length scale 0.9 and amplitude 0.92, and  $\kappa^{\tau}$  is a Matern-3/2 kernel with length scale 1.2. The particular values of the length scales / amplitudes are of little importance to the proof-of-concept experiments presented in this work – they were chosen pseudo-randomly.

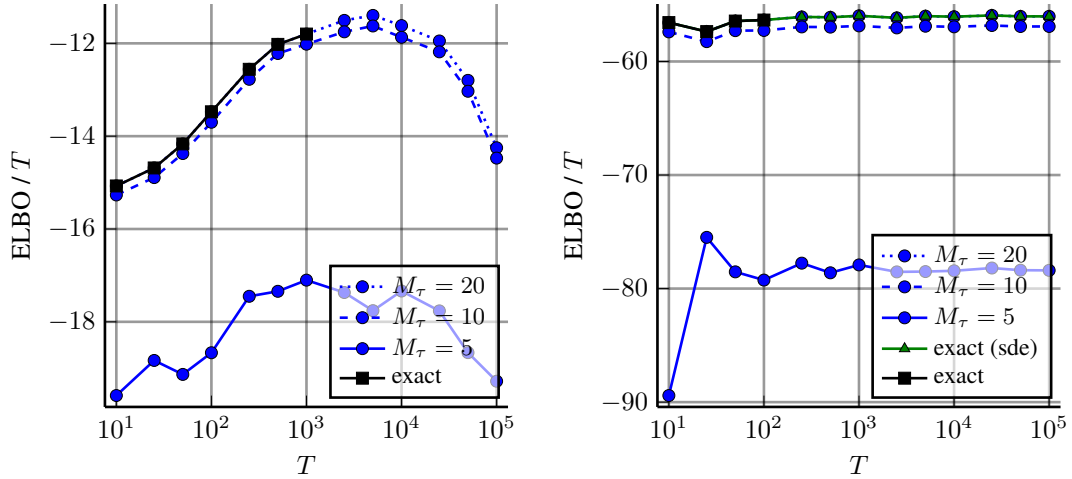


Figure 11: The ELBO obtained vs the exact LML. The bound appears reasonably tight when  $M_\tau = 10$  are used per time point, and very tight for  $M_\tau = 20$ .  $M_\tau = 5$  is clearly insufficient.

These experiments were conducted using a single thread on a 2019 MacBook Pro with 2.6 GHz CPU. Timings produced using benchmarking functionality provided by Chen and Revels [2016].

#### E.1.1 Sum-Separable Experiments

Similar experiments to those in section Sec. 6 were performed with the sum-separable kernel given by adding two separable kernels of the form in Eq. (1), although with similar length-scales and amplitudes. The results are broadly similar, although the state space approximations and state space + pseudo-point approximations take a bit longer to run as there are twice as many latent dimensions for a given number of pseudo-points than in the separable model. As before, these experiments should be thought of purely as a proof of concept.

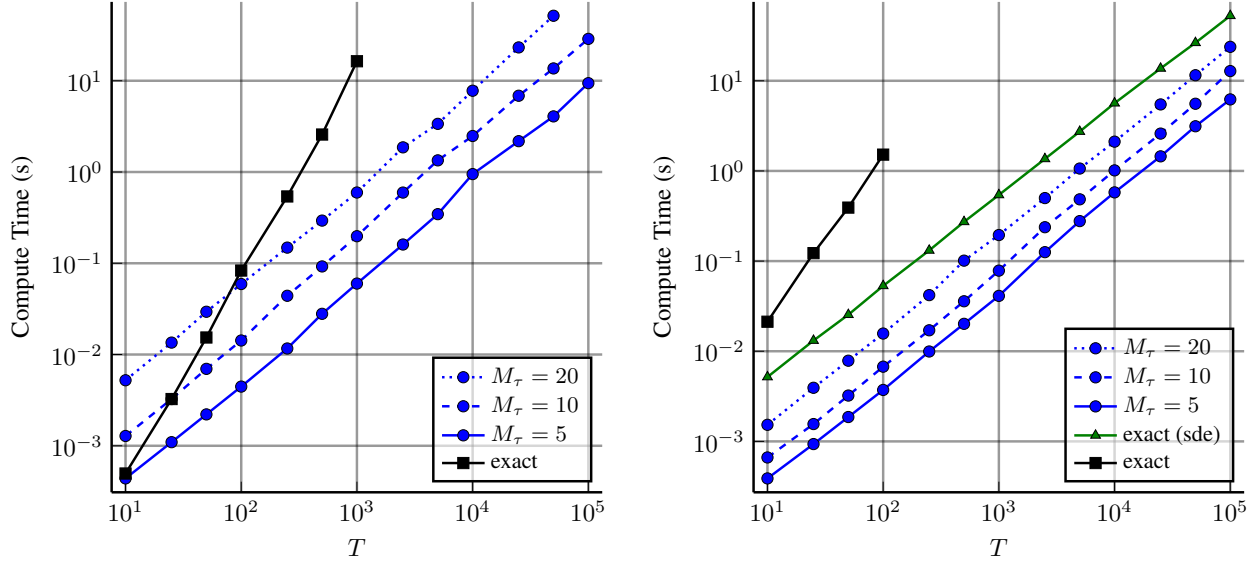


Figure 12: Time to compute LML exactly vs ELBO with a sum of two separable kernels. Left: irregular samples as per Fig. 4. Right: regular samples with missing data as per Fig. 5. Observe that, due to the increased latent dimensionality of the sum-separable model, it takes longer to compute the ELBO (and LML using the vanilla state space approximation) than in the separable case.

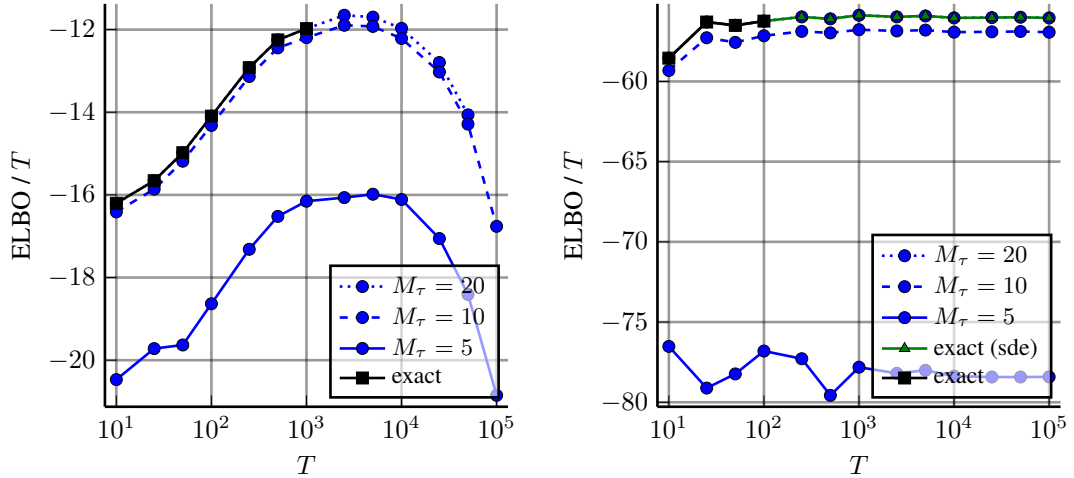


Figure 13: Analogue of Fig. 11 for Fig. 12. As before,  $M_\tau = 5$  is clearly insufficient for accurate inference, while  $M_\tau = 20$  is very close to the LML.

## E.2 CLIMATOLOGY DATA

The spatial locations of the pseudo-points were chosen via k-means clustering of lat-lon coordinates of sold apartments, using Clustering.jl, and were not optimised beyond that.<sup>1</sup>

The separable kernel was

$$\kappa((\mathbf{r}, \tau), (\mathbf{r}', \tau')) = s \kappa_{\mathbf{r}}(\Lambda \mathbf{r}, \Lambda \mathbf{r}') \kappa_{\tau}(\lambda \tau, \lambda \tau') \quad (75)$$

where  $\kappa_{\tau}$  is a standardised Matérn- $\frac{5}{2}$ ,  $\kappa_{\mathbf{r}}$  is a standardised Exponentiated Quadratic,  $\Lambda$  is a diagonal matrix with positive elements,  $\lambda > 0$ ,  $s > 0$ . Initialisation:  $\lambda = 10^{-2}$ ,  $\Lambda_{d,d} = 1$ ,  $s = 1$ ,  $d \in \{1, 2, 3\}$ . Observation noise variance initialised to 0.5.

The L-BFGS implementation provided by Mogensen and Riseth [2018] was utilised to optimise the ELBO, with memory  $M = 50$  iterations, and gradients computed using the Zygote.jl algorithmic differentiation tool [Innes, 2018]. All kernel parameters constrained to be positive by optimising the log of their value, and observation noise variance constrained to be in  $[10^{-2}, 2]$  via a re-scaled logit transformation – this is justifiable as the data itself was standardised to have unit variance.

The sum-separable model comprises a sum of two GPs with kernels of this form. Initialisation:  $\lambda = \{10^{-3}, 10^{-1}\}$ ,  $\Lambda_{d,d} = \{1.0, 5.0\}$ ,  $s = \{0.7, 0.3\}$ . The same optimisation procedure was used.

## E.3 APARTMENT DATA

The spatial locations of the pseudo-points were chosen via k-means clustering of lat-lon coordinates of sold apartments, using Clustering.jl, and were not optimised beyond that.  $M_{\tau} = 75$  pseudo-points used per time point.

The separable kernel was

$$\kappa((\mathbf{r}, \tau), (\mathbf{r}', \tau')) = s \kappa_{\mathbf{r}}(\Lambda \mathbf{r}, \Lambda \mathbf{r}') \kappa_{\tau}(\lambda \tau, \lambda \tau') \quad (76)$$

where  $\kappa_{\tau}$  is a standardised Matérn- $\frac{3}{2}$ ,  $\kappa_{\mathbf{r}}$  is a standardised Exponentiated Quadratic,  $\Lambda$  is a diagonal matrix with positive elements,  $\lambda > 0$ ,  $s > 0$ . Initialisation:  $\lambda = 10^{-2}$ ,  $\Lambda_{d,d} = 1$ ,  $s = 1$ ,  $d \in \{1, 2\}$ . Observation noise variance initialised to 0.5.

The L-BFGS implementation provided by Mogensen and Riseth [2018] was utilised to optimise the ELBO, with memory  $M = 50$  iterations, and gradients computed using the Zygote.jl algorithmic differentiation tool [Innes, 2018]. All kernel parameters constrained to be positive by optimising the log of their value, and observation noise variance constrained to be in  $[10^{-2}, 2]$  via a re-scaled logit transformation – this is justifiable as the data itself was standardised to have unit variance.

The sum-separable model comprises a sum of two GPs with kernels of this form. Initialisation:  $\lambda = \{10^{-3}, 10^{-1}\}$ ,  $\Lambda_{d,d} = \{1.0, 5.0\}$ ,  $s = \{0.7, 0.3\}$ . The same optimisation procedure was used.

## F EFFICIENT INFERENCE IN LINEAR LATENT GAUSSIAN MODELS

Consider the linear-Gaussian model

$$\begin{aligned} \mathbf{x} &\sim \mathcal{N}(\mathbf{m}_{\mathbf{x}}, \mathbf{C}_{\mathbf{x}}) \\ \mathbf{y} \mid \mathbf{x} &\sim \mathcal{N}(\mathbf{A}\mathbf{x} + \mathbf{a}, \mathbf{Q}) \end{aligned}$$

where  $\mathbf{m}_{\mathbf{x}} \in \mathbb{R}^{D_x}$  and  $\mathbf{a} \in \mathbb{R}^{D_y}$  are vectors,  $\mathbf{C}_{\mathbf{x}}$  is a  $D_x \times D_x$  positive-definite matrix,  $\mathbf{Q}$  is a  $D_y \times D_y$  diagonal positive definite matrix, and  $\mathbf{A}$  is a  $D_y \times D_x$  matrix. We need to

1. generate samples from the marginal distribution over  $p(\mathbf{y})$ ,
2. compute the marginals  $p(\mathbf{y}_n)$ ,  $n = 1, \dots, D_y$ ,
3. compute the LML  $p(\mathbf{y})$ , and
4. compute the posterior distribution  $p(\mathbf{x} \mid \mathbf{y})$ .

All of these operations can be performed exactly in polynomial-time since  $\mathbf{x}$  and  $\mathbf{y}$  are jointly Gaussian distributed. However, there are two approaches for computing 1, 3, and 4, one of which will be faster depending upon  $D_x$  and  $D_y$ .

In this section we analyse these approaches. We do this to prepare for deriving the additional algorithms needed to perform the above operations efficiently when  $\mathbf{A} := \mathbf{BC}$ , for tall  $\mathbf{B}$  and wide  $\mathbf{C}$ .

<sup>1</sup><https://github.com/JuliaStats/Clustering.jl>

## F.1 PRELIMINARIES

The marginal distribution over  $\mathbf{y}$  is

$$\mathbf{y} \sim \mathcal{N}(\mathbf{m}_y, \mathbf{C}_y), \quad \mathbf{m}_y := \mathbf{A}\mathbf{m}_x + \mathbf{a}, \quad \mathbf{C}_y := \mathbf{A}\mathbf{C}_x\mathbf{A}^\top + \mathbf{Q}.$$

Computing  $\mathbf{A}\mathbf{C}_x$  requires  $\mathcal{O}(D_y D_x^2)$  operations, and  $(\mathbf{A}\mathbf{C}_x)\mathbf{A}^\top$  requires  $\mathcal{O}(D_y^2 D_x)$ , so constructing the marginals takes roughly  $\mathcal{O}(D_y D_x^2 + D_y^2 D_x)$  operations.

By computing  $p(\mathbf{y})$  we will mean computing  $\mathbf{m}_y$  and  $\mathbf{C}_y$ .

## F.2 SAMPLING

First consider sampling from the marginal distribution over  $p(\mathbf{y})$ . The two approaches to this are:

1. Ancestral sampling: first sample from  $p(\mathbf{x})$  then from  $p(\mathbf{y} | \mathbf{x})$ .
2. Direct marginal sampling: compute the marginal distribution  $p(\mathbf{y})$  and sample from it directly.

Ancestral sampling requires computing the Cholesky factorisation of  $\mathbf{C}_x$ , thus the overall algorithm requires  $\mathcal{O}(D_x^3 + D_x D_y)$  scalar operations. Conversely, computing  $p(\mathbf{y})$  and sampling from it requires  $\mathcal{O}(D_y D_x^2 + D_y^2 D_x + D_y^3)$  scalar operations. So if  $D_x$  is much smaller than  $D_y$  we are better off using ancestral sampling, but if  $D_x$  is much larger than  $D_y$  then direct marginal sampling is better.

## F.3 COMPUTING MARGINAL PROBABILITIES

To compute all  $p(\mathbf{y}_n)$  we must compute both  $\mathbf{m}_y$  and the diagonal of  $\mathbf{C}_y$ .  $\mathbf{m}_y$  requires only  $\mathcal{O}(D_x D_y)$  scalar operations. Once  $\mathbf{A}\mathbf{C}_x$  has been computed, obtaining the diagonal of  $\mathbf{C}_y$  requires only an additional  $\mathcal{O}(D_x D_y)$  scalar operations, so the whole operation requires roughly  $\mathcal{O}(D_y D_x^2)$  operations.

## F.4 COMPUTING THE LOG MARGINAL LIKELIHOOD AND POSTERIOR

These two operations can be performed separately, but it typically makes sense to perform them together as the majority of computational work is shared between them.

---

**Algorithm 1** LML by and posterior by factorising  $p(\mathbf{y})$ . Approx. number of scalar operations on the right of each line.

---

1: <b>Naive-Inference:</b> $\mathbf{m}_x, \mathbf{C}_x, \mathbf{A}, \mathbf{a}, \mathbf{Q}, \mathbf{y}$	
2: $\mathbf{V} \leftarrow \mathbf{A}\mathbf{C}_x$	$\mathcal{O}(D_y D_x^2)$
3: $\mathbf{C}_y \leftarrow \mathbf{V}\mathbf{A}^\top + \mathbf{Q}$	$\mathcal{O}(D_y^2 D_x)$
4: $\mathbf{U} \leftarrow \text{cholesky}(\mathbf{C}_y)$	$\mathcal{O}(D_y^3)$
5: $\mathbf{B} \leftarrow \mathbf{U}^{-\top} \mathbf{V}$	$\mathcal{O}(D_y^2 D_x)$
6: $\alpha \leftarrow \mathbf{U}^{-\top} (\mathbf{y} - (\mathbf{A}\mathbf{m}_x + \mathbf{a}))$	$\mathcal{O}(D_y^2)$
7: $\text{lml} \leftarrow -\frac{1}{2} [D_y \log 2\pi + 2 \log \det \mathbf{U} + \alpha^\top \alpha]$	$\mathcal{O}(D_y)$
8: $\mathbf{m}_{x y} \leftarrow \mathbf{m}_x + \mathbf{B}^\top \alpha$	$\mathcal{O}(D_y D_x)$
9: $\mathbf{C}_{x y} \leftarrow \mathbf{C}_x + \mathbf{B}^\top \mathbf{B}$	$\mathcal{O}(D_x^2 D_y)$
10: <b>return</b> $\mathbf{m}_{x y}, \mathbf{C}_{x y}, \text{lml}$	

---



---

**Algorithm 2** LML and posterior by exploiting the matrix inversion and determinant lemmas. Approx. number of scalar operations on the right of each line. Note that since  $\mathbf{Q}$  is diagonal, its Cholesky factorisation is also diagonal.

---

```

1: Low-Rank-Inference:  $\mathbf{m}_x, \mathbf{C}_x, \mathbf{A}, \mathbf{a}, \mathbf{Q}, \mathbf{y}$ 
2:  $\mathbf{U}_Q \leftarrow \text{cholesky}(\mathbf{Q})$   $\mathcal{O}(D_y)$ 
3:  $\mathbf{U}_x \leftarrow \text{cholesky}(\mathbf{C}_x)$   $\mathcal{O}(D_x)$ 
4:  $\mathbf{B} \leftarrow \mathbf{U}_x \mathbf{A}^\top \mathbf{U}_Q^{-1}$   $\mathcal{O}(D_x^2 D_y)$ 
5:  $\mathbf{U} \leftarrow \text{cholesky}(\mathbf{B}\mathbf{B}^\top + \mathbf{I})$   $\mathcal{O}(D_x^3 + D_x^2 D_y)$ 
6:  $\mathbf{G} \leftarrow \mathbf{U}^{-\top} \mathbf{U}_x$   $\mathcal{O}(D_x^3)$ 
7:  $\mathbf{C}_{x|y} \leftarrow \mathbf{G}^\top \mathbf{G}$   $\mathcal{O}(D_x^3)$ 
8:  $\delta \leftarrow \mathbf{U}_Q^{-\top} (\mathbf{y} - (\mathbf{A}\mathbf{m}_x + \mathbf{a}))$   $\mathcal{O}(D_y)$ 
9:  $\beta \leftarrow \mathbf{B}\delta$   $\mathcal{O}(D_y D_x)$ 
10:  $\mathbf{m}_{x|y} \leftarrow \mathbf{m}_x + \mathbf{G}^\top (\mathbf{U}^{-\top} \beta)$   $\mathcal{O}(D_x^2)$ 
11:  $\text{lml} \leftarrow -\frac{1}{2} [\delta^\top \delta - (\mathbf{U}^{-\top} \beta)^\top \mathbf{U}^{-\top} \beta + D_y \log 2\pi + 2 \log \det \mathbf{U} + 2 \log \det \mathbf{Q}]$   $\mathcal{O}(D_x^2)$ 
12: return  $\mathbf{m}_{x|y}, \mathbf{C}_{x|y}, \text{lml}$ 

```

---

Note that Algorithm 1 and Algorithm 2 are locally scoped, so the symbols don't necessarily correspond to the same quantities. For example,  $\mathbf{B}$  is different in each algorithm.

## F.5 BOTTLENECK LINEAR-GAUSSIAN OBSERVATION MODELS

The above inference methods assume no particular structure in  $\mathbf{A}$ , however, recall that Eq. (23) gives  $\mathbf{A}$  at time  $t$  to be

$$\mathbf{A} = \mathbf{C}_{\mathbf{f}_{n,t}, \mathbf{u}_t} \Lambda_{\mathbf{u}_t} \mathbf{H}_{\mathbf{u}} \quad (77)$$

where  $\mathbf{H}_{\mathbf{u}}$  is  $M \times MD$  and  $\mathbf{C}_{\mathbf{f}_{n,t}, \mathbf{u}_t}$  is  $N \times M$ . Most kernels have  $D > 1$ , so it's worth determining whether we can exploit this structure to accelerate inference.

To this end consider a model given by

$$\mathbf{z} := \mathbf{H}\mathbf{x} + \mathbf{h}, \quad \mathbf{x} \sim \mathcal{N}(\mathbf{m}_x, \mathbf{C}_x) \quad (78)$$

$$\mathbf{y} := \mathbf{B}\mathbf{z} + \mathbf{b} + \varepsilon, \quad \varepsilon \sim \mathcal{N}(\mathbf{0}, \mathbf{Q}) \quad (79)$$

where  $\mathbf{H} \in \mathbb{R}^{M \times DM}$ ,  $\mathbf{h} \in \mathbb{R}^M$ ,  $\mathbf{B} \in \mathbb{R}^{N \times M}$ ,  $\mathbf{b}, \varepsilon \in \mathbb{R}^N$ , and  $\mathbf{Q} \in \mathbb{R}^{N \times N}$  is a positive-definite diagonal matrix. We call this a *bottleneck* model, since  $\mathbf{z}$  carries all of the information in  $\mathbf{x}$  needed to perform inference in  $\mathbf{y}$ , its dimension is less than that of  $\mathbf{x}$  and  $\mathbf{y}$  in the problems that we consider.

Observe that this model forms a two-state degenerate Markov chain. Algorithm 3 exploits this Markov structure, and is able to recycle Algorithm 2 as a consequence. It comprises three broad components: computing the marginals over  $\mathbf{z}$ , computing the posterior  $\mathbf{z}|\mathbf{y}$ , and finally computing the posterior  $\mathbf{x}|\mathbf{y}$ . This last step is equivalent to performing a single step of RTS smoothing.

---

**Algorithm 3** LML and posterior. Exploits the matrix inversion and determinant lemmas, and the bottlenecked structure of the model. Approx. number of scalar operations on the right of each line.

---

```

1: Bottleneck-Inference:  $\mathbf{m}_x, \mathbf{C}_x, \mathbf{B}, \mathbf{b}, \mathbf{Q}, \mathbf{H}, \mathbf{h}, \mathbf{y}$ 
2:  $\mathbf{m}_z \leftarrow \mathbf{H}\mathbf{m}_x + \mathbf{h}$   $\mathcal{O}(D_z D_x)$ 
3:  $\mathbf{C}_z \leftarrow \mathbf{H}\mathbf{C}_x\mathbf{H}^\top + \mathbf{I}$   $\mathcal{O}(D_z D_x^2 + D_z^2 D_x)$ 
4:  $\mathbf{m}_{z|y}, \mathbf{C}_{z|y}, \text{lml} \leftarrow \text{Low-Rank-Inference}(\mathbf{m}_z, \mathbf{C}_z, \mathbf{B}, \mathbf{b}, \mathbf{Q})$   $\mathcal{O}(D_z^2 D_y + D_z^3)$ 
5:  $\mathbf{U} \leftarrow \text{cholesky}(\mathbf{C}_{z|y})$   $\mathcal{O}(D_z^3)$ 
6:  $\mathbf{G} \leftarrow \mathbf{C}_x \mathbf{H}^\top \mathbf{U}^{-1} \mathbf{U}^{-\top}$   $\mathcal{O}(D_x^2 D_z)$ 
7:  $\mathbf{m}_{x|y} \leftarrow \mathbf{m}_x + \mathbf{G}^\top (\mathbf{m}_{z|y} - \mathbf{m}_z)$   $\mathcal{O}(D_z D_x)$ 
8:  $\mathbf{C}_{x|y} \leftarrow \mathbf{C}_x + \mathbf{G}^\top (\mathbf{C}_{z|y} - \mathbf{C}_z) \mathbf{G}$   $\mathcal{O}(D_z^2 D_x + D_x^2)$ 
9: return  $\mathbf{m}_{x|y}, \mathbf{C}_{x|y}, \text{lml}$ 

```

---

Observe that this algorithm exchanges  $\mathcal{O}(D_x^3)$  for  $\mathcal{O}(D_z^3)$  operations. Recalling that  $D_x = MD$  and  $D_z = M$ , we expect that this algorithm will produce better performance than Algorithm 2 for some value of  $D > 1$ . Since the exact value of  $D$

at which this change will occur is unclear, and the optimal choice of algorithm for the experiments in this work depends on this, we investigate the effect of  $D$ ,  $M$ , and  $N$  on the performance of each algorithm in the next subsection.

## F.6 BENCHMARKING INFERENCE

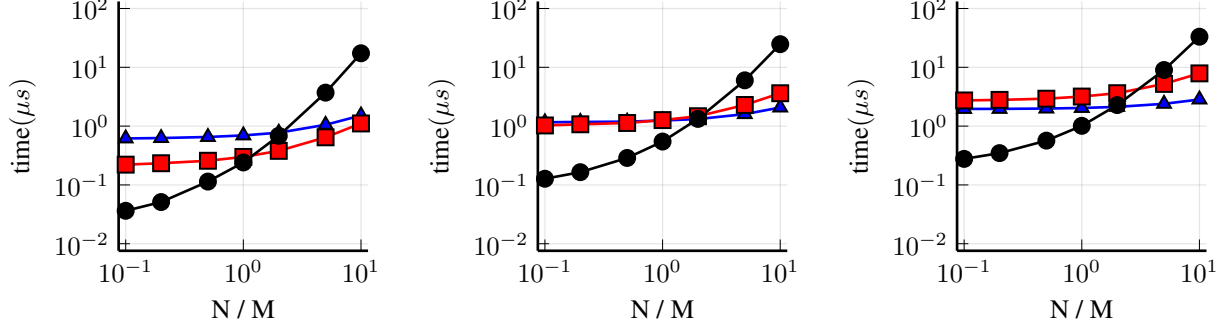


Figure 14: Black-circle=naive, red square=low rank, blue triangle=bottleneck. All experiments conducted using  $M = 100$  pseudo-points. Left:  $D = 1$ , Middle:  $D = 2$ , Right:  $D = 3$ .

Fig. 14 shows the performance of the three different algorithms for computing the LML and posterior distribution as the dimensions of the linear-Gaussian model’s dimensions change. Black lines with circles use Algorithm 1 (labelled *naive*), red lines with squares used Algorithm 2 (labelled *low rank*), and blue lines with triangles use Algorithm 3 (labelled *bottleneck*). The experiments are set up to match situations encountered in the spatio-temporal models discussed in this paper – they are parametrised in terms of the number of  $M$ ,  $N$ , and  $D$ .  $M$  is fixed to 100 across all three graphs, the total number of latent dimensions is  $MD$  for  $D \in \{1, 2, 3\}$ , corresponding to the Matérn-1/2, Matérn-3/2, and Matérn-5/2 kernels respectively. The number of observations  $N$  range between  $0.1M = 10$  and  $10M = 1000$ .

As expected the *naive* algorithm performs better when  $N < M$ , but this quickly changes when  $N > M$ . For the kinds of problems encountered in this work we generally have that  $N > M$ , which would suggest that correct choice in our work is typically the *low-rank* algorithm. For  $M = N$  the *naive* algorithm tends to be faster, owing to the smaller number of operations used – it’s just a shorter algorithm than the *low-rank* algorithm.

Algorithm 3, *bottleneck*, performs similarly or better than Algorithm 2 for  $D = 2$  and  $D = 3$ . The gap between the two grows as  $N$  grows, suggesting that Algorithm 3 will typically be a better choice for large  $M$ . Indeed, even for  $D = 1$  the difference between the two becomes close for large  $N$ .

Given that  $N$ ,  $M$  and  $D$  determine which of the three algorithms is optimal, one must choose appropriately for any given application. We adopt the bottleneck algorithm in all experiments in this work because we consistently work in regimes where  $N > M$  at most points in time, and we do not make use of any kernels for which  $D = 1$ .

Also note that these results highlight that using Algorithm 2 to perform the second step in Algorithm 3 is only optimal if  $N > M$ . If a problem were encountered for which  $N < M$  it would be prudent to consider replacing it with Algorithm 1.